Advancements in terahertz-enabled photoconductive antenna design: a review

Ruobin Han[1] (iD), Abdoalbaset Abohmra[1], Tomas Pires[1], Joao Ponciano[1], Hasan Abbas[1], Akram Alomainy[2], Farooq Ahmad Tahir[1,3] (iD), Muhammad Imran[1] and Qammer Abbasi[1,4]

[1]James Watt School of Engineering, University of Glasgow, Glasgow, UK; [2]School of Electronic Engineering and Computer Science, Queen Mary University of London, London, UK; [3]School of Electrical Engineering and Computer Science (SEECS), National University of Sciences and Technology, Islamabad, Pakistan and [4]Artificial Intelligence Research Centre, Ajman University, Ajman, UAE

Abstract

Photoconductive antennas (PCAs), known for their broad bandwidth, high data rates, and simple structure, are gaining significant attention in terahertz (THz) applications. Over the past decade, THz PCAs have been extensively researched, demonstrating diverse applications across multiple fields. This paper provides a comprehensive review of PCA theory and design, along with an in-depth analysis of their relative advantages. Additionally, various strategies for enhancing antenna efficiency are discussed, focusing on material selection and geometric design. This review aims to offer researchers a consolidated resource, presenting key insights into the challenges and advancements in PCA research.

CAMBRIDGE UNIVERSITY PRESS

Introduction of THz technologies

Terahertz (THz) wave is located between the optical frequency region and microwave frequency region in the electromagnetic wave spectrum, covering the frequency range between 0.1 and 10 THz with the wavelength of 3 mm to 30 μm [1]. An overview of THz frequency region is illustrated in Fig. 1. Radiation of this frequency is nonionizing. Thus, it is identified as a much safer alternative to conventional ionizing radiation techniques used in medical diagnoses, such as CT scans and X-rays. The energy of a single photon in THz waves is significantly less than that of X-rays, approximately one millionth of the energy of X-ray photons [2]. This gives a bright future to THz technology in the biomedical field, such as T-ray scanning used in pharmaceutical settings and skin cancer diagnoses [3–6]. THz waves can penetrate various objects, including wood, plastic, fabric, leather, paper, and, most importantly, human skin [7]. It provides great potentiality in novel sensing and imaging possibilities [8–19].

However, despite the research on THz antennas, the current study on PCA is not yet mature. Although the theory of PCA is getting more exceptional, there appears to be a practical knowledge gap in efficiency and gain. There is a lack of joint research on efficiency and gain improvement in the prior literature of PCA enhancement, among which there is only the comparison of conventional substrates and research on various photoconductive materials, or only novel structures of substrates are mentioned. Current work studies and summarizes all the proven enhancement methods for efficiency and gain of PCA in the last decade, with detailed theoretical research and formula expressions. Relative research on silicon meta-lens [20, 21], plasmonic nanostructures [22–25], large area photoconductive nanoantenna arrays [26–31], dielectric superstrate [32–35], and photonic crystal structures [36–41] have been put forward in recent years. Also, this paper reviews several challenges and gives a brief overview of the PCA enhancement study, providing a concise direction of THz PCA technology for the next few years.

Theory of THz PCA

Physics

A PCA includes a photoconductive substrate and a set of antenna conductors, often consisting of a pair of DC-biased electrodes. The electrodes are usually metal dipoles with an antenna gap. The electrodes are patterned on the photoconductor, while the gap is positioned at the center of the substrate. The radiation performance of PCA is affected by three factors: the material composition of the photoconductive substrate, the geometry design of the antenna, and the femtosecond laser pulse. Current technology can produce a laser pulse of femtosecond levels, and
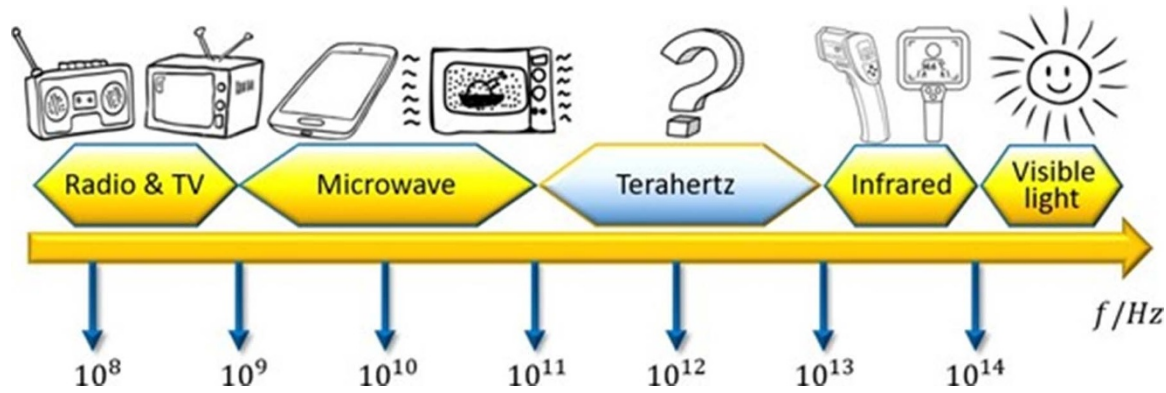
Figure 1. The THz frequency band is positioned between the microwave region and the optical region of the electromagnetic spectrum.

the antenna geometry is continuing to innovate. In this paper, research on material and novel geometric structures is reviewed.

Regarding the study of photoconductive materials, substrate materials should possess shorter carrier lifetime, higher resistivity, and faster carrier mobility to meet the general requirements [42]. Thus, many researchers used GaAs, GaP, and ZnTe in various designs [43, 44]. When a PCA is excited, the laser pulses are focused on the center gap, with which the energy propagates into the photoconductor and is absorbed by the substrate; thus, transient photocurrent is produced by the accelerated photo carriers. In most studies, 800 and 1550 nm wavelength laser pulses are used to feed PCA in experiments [45, 46]. Figure 2(a) illustrates the process by which the transient photocurrent produced in the photoconductor drives the antenna and eventually leads to the emission of THz pulses. The PCA transient response is depicted in Figs. 2(b–e) [19]. When a light pulse is absorbed in a photoconductor, the generation of charge carriers is proportional to light. The photo carriers are accelerated along the DC field and produce a transient photocurrent whose rise time approaches the incident light rise time. The decay time following the peak of the photocurrent is determined by the properties of the photoconductive substrate instead of the temporal distribution of light. If the duration of the carriers of the photoconductor is short, the carriers produced by the optical pulse initiate the recombination process immediately following the absorption of the pulse.

On the other hand, if the substrate material possesses a long carrier lifetime, the resulting carriers will continue to contribute photocurrent after the light pulse is completely absorbed. This causes an increase in the photocurrent pulse, leading to a corresponding enlargement in the output pulse and a decrease in the overall bandwidth of the THz frequency. To circumvent this problem, photoconductive materials with subpicosecond duration are typically utilized. The selection of materials will be discussed in the next section.

Key challenges in THz PCA

Although PCA is prospective due to its simple structure and tiny size, current research is not solving the problem of the low convention efficiency from laser to THz waves. Also, the free space path loss (FSPL) of THz waves is high. Thus, it can hardly cover a distance further than 10 m. The path loss can be computed by the Friis transmission equation [47]:

$$FSPL = 20 \log \left(\frac{4\pi d}{\lambda} \right) [dB] \quad (1)$$

where d represents the distance and λ represents the wavelength. In accordance with the Friis equation, the THz band has a higher path loss due to its high frequency. This is because the molecule absorption loss leads to multiple degrees of high attenuations [48].

The efficiency of PCA comprises two factors—radiation efficiency and impedance matching efficiency, which are defined as [49]

$$\eta_r = \frac{P_r}{P_{in}}, \ \eta_m = \frac{P_{in}}{P_s} \quad (2)$$

These equations indicate that efficiency is defined by the ratio of the radiated power Pr to the input power Ps. The total efficiency of PCA is [49]

$$\eta_t = \eta_m \eta_r = P_r / P_s \quad (3)$$

Thus, the optical-to-THz conversion efficiency of PCA is determined by the ratio of the laser power focusing on the PCA gap to the power of radiated THz signals. A study by Goldsmith [50] approximated the laser-to-electrical efficiency as follows:

$$\eta_{LE} = \frac{P_E}{P_L} \approx \frac{eV_b^2 \mu \tau^2 \eta_L f_R}{h f_L l^2} \quad (4)$$

In the above equation, e and μ correspond to the electron charge and mobility, Vb represents the applied bias voltage, τ signifies the decay time of the photocurrent, ηL denotes the illumination efficiency, fR and fL refer to the repetition rate and frequency of the laser, respectively, while l represents the length of the PCA gap.

Two challenging issues to be investigated in this area are laser-to-electrical efficiency and the gain enhancement due to a high loss of THz pulses. Different studies to improve efficiency and gain are studied in this paper, including the fields of geometric structures, substrate materials, and new technologies.

PCA efficiency and gain enhancement

The radiation of the PCA primarily depends on the following three factors: the material of the photoconductive substrate and antenna, the geometry structure of the antenna, and the femtosecond laser pulse. The current research in THz PCA designs has proved that it can be a promising technology for future use and can be applied in numerous fields of communication, such as medical imaging, spectroscopy, and security. However, because of the low optical-to-THz conversion efficiency and substantial material loss, a severe challenge is to improve efficiency and realized gain. Here, various studies are reviewed to summarize methods that improve PCA efficiency and gain.

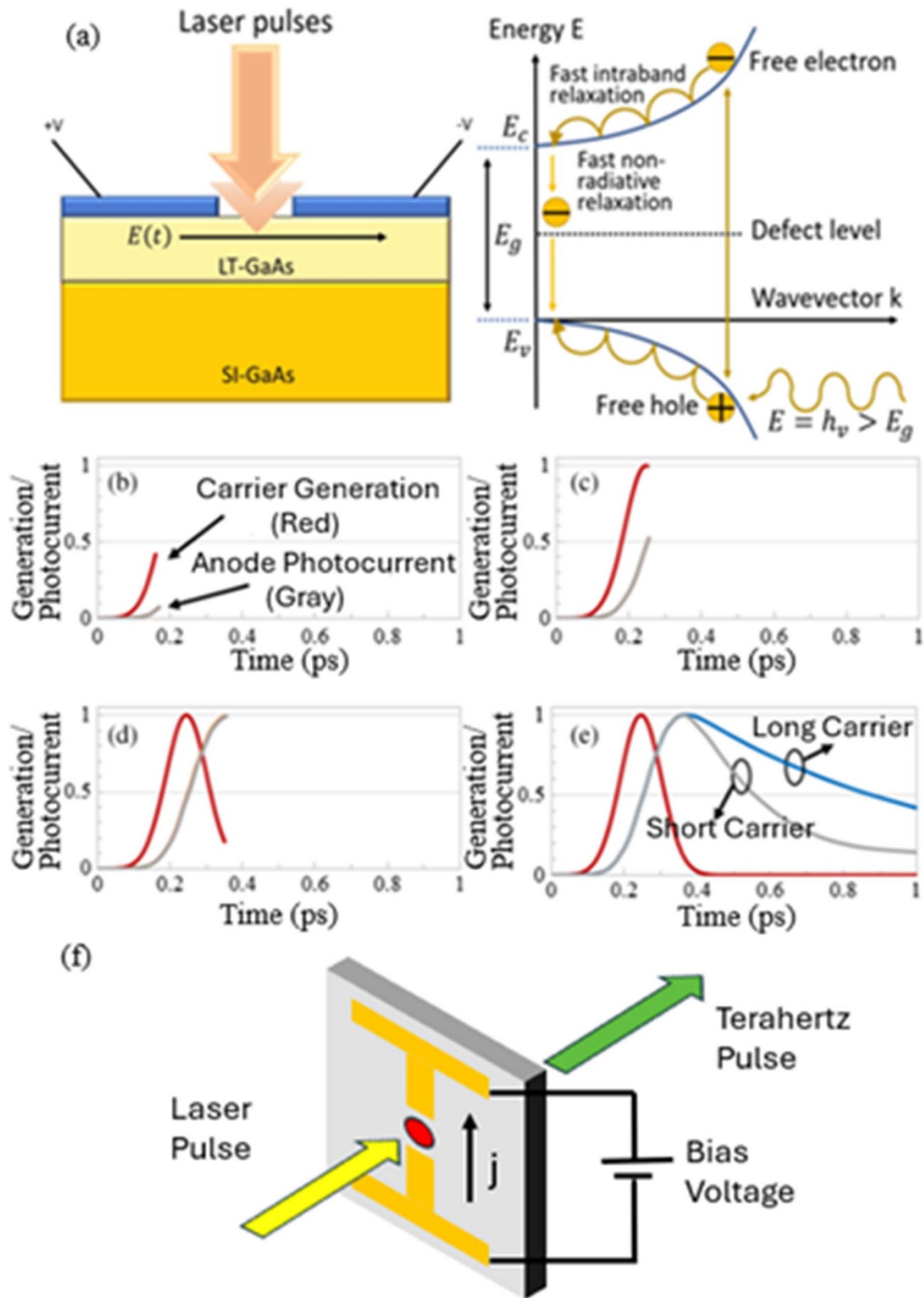**Figure 2.** (a) The excitation of PCA by laser; (b–e) generation of photocurrent in semiconductors (red trace) and photocurrent in the antenna gap for the photoconductive material for long carrier lifetime and short carrier lifetime, represented by gray and blue trace, respectively [19]; (f) Illustration of a PCA. Bias voltage is applied to both electrodes and surface current is generated on the substrate.

Table 1. Carrier lifetimes of LT-GaAs at different growth temperatures, and the nature of three types of GaAs material

Growth temperature (°C)	Carrier lifetime (ps)
175	0.18−0.38 [60]
200	0.325−0.425 [60]
225	0.4−0.5 [60]
250	0.61−0.71 [60]
300	1.3 [61]

Table 2. Comparison of the properties of LT-GaAs, SI-GaAs, and LT-InGaAs

Material	SI-GaAs	LT-GaAs	LT-InGaAs
Carrier lifetime (ps)	Several hundred [64]	<1.4 [58, 65]	Larger than LT-GaAs [66]
Mobility ($cm^2 \cdot V^{-1} \cdot s^{-1}$)	8500 [67]	200 [64]	26 [68]
Resistivity ($\Omega \cdot cm$)	$\approx 10^7$ [69]	$>10^7$ [56]	760 [68]
Breakdown field ($V \cdot cm^{-1}$)	4×10^5 [67]	5×10^5 [64]	$\approx 6 \times 10^4$ [68]

Materials

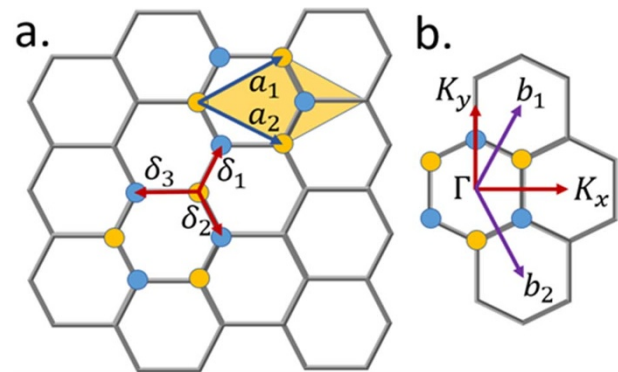### Photoconductive materials of substrates and electrodes

In the past decades, the development in physics and material science has significantly been beneficial to the research in the antenna field. Several suitable photoconductive materials have been used in the design and fabrication of the THz PCA. To obtain high optical-to-THz conversion, a low-loss photoconductive-dielectric material is always required. Photoconductivity is an essential characteristic of THz signal generation; thus, the researchers choose III–V compound semiconductors like GaAs, SI-GaAs (Semi-insulting GaAs), and InGaAs (Indium Gallium Arsenide) in designs, among which the most widely obtained material is LT-GaAs (Low-Temperature Grown GaAs) [51]. According to research conducted by [52], in the absence of natural materials capable of transmitting THz waves with satisfactory efficiency, III–V compound semiconductors such as GaAs favored over other materials for THz wave generation due to their ability to optimize electrical and optical properties by manipulating their composition. GaAs, in particular, possess a bandgap of 1.424 eV at normal temperature [53], which is compatible with commonly used titanium-doped sapphire (Ti^{3+}:sapphire) femtosecond pulse sources used to stimulate PCAs [54, 55]. The use of LT-GaAs as a substrate for THz PCAs was first introduced in 1988 [56]. LT-GaAs grown at 250°C via molecular beam epitaxy exhibits high crystallinity, resulting in increased carrier mobility, and excess As^{3+} within the crystal structure, leading to point defects [57]. LT-GaAs that grow at 200°C is proven to have a lifetime of around 0.4 ps [58], while 250°C LT-GaAs is found to have 0.7 ps lifetime carrier [59], indicating that the carrier lifetimes are higher once the temperature improves in LT scale. Table 1 shows the measured lifetimes of LT-GaAs by different research due to the growth temperature [60].

However, errors in the carrier lifetime measurement are unavoidable. During the last 30 years, the physical properties of GaAs have been studied and measured, and different measured results of the LT-GaAs carrier lifetime have been published. Taking 250°C as the example, in research of [60], LT-GaAs grown at this temperature has a carrier lifetime of 0.66 ± 0.05 ps. It is also shown that GaAs carrier lifetimes with this temperature are 0.25 ps [62], 0.7 ps [61], 1 ps [63], and 1.4 ps [61]. The InGaAs is also used as photoconductive substrates; however, it has different mobility and resistivity. Table 2 shows the comparison of the properties of these three photoconductive compounds. Overall, LT-GaAs is regarded as the most favorable photoconductive material obtained in PCA studies due to its exceptional combination of characteristics.

In most antenna designs, copper, gold, and other extremely conductive metal materials are used for electrodes. In THz PCA design, Au (gold), Ti (titanium), and stacked Ti-Au structure are used more [70, 71]. Au has a conductivity of 45.2×10^6 S/m, and

Figure 3. (a) A depiction of the hexagonal structure of graphene, with unit vectors a1 and a2 indicating the sublattice and two atoms per cell. The distance between every two closest atoms is represented by δ. The lattice vectors are shown as blue arrows. (b) b1 and b2 stand for the reciprocal lattice vectors at the Brillouin zone.

by $\delta = \left(\frac{1}{\pi f \mu \sigma} \right)^{\frac{1}{2}}$, the skin depth is 74.9 nm at 1 THz frequency [1]. In the Ti-Au structure, the stickiness of Au is improved by assimilating Ti sheets, so that the connection of electrodes and substrates is compact and stable [72]. Also, no annealing is required after deposition in the Ti-Au fabrication process [73]. Therefore, in the process of PCA design, simulation, and fabrication, the electrodes often consist of Au with tens of nanometers thickness and a 10–20 nm Ti layer.

Key challenges for lower bandgap materials include achieving carrier lifetimes, mobilities, breakdown thresholds, quantum efficiencies, and reproducibility levels comparable to or surpassing those of conventional photoconductive materials. In this case, GaAs and relevant III–V compound semiconductors continue to be the benchmark material for THz PCAs in the past, current, and future optoelectrical research.

Graphene-based PCA design

Graphene is another material that can potentially be the solution of PCA performance enhancement, with 1.5 Tpa Young's modulus, 24×10^4 cm^{-1} absorption coefficient, and 2×10^5 cm^2 V^{-1} s^{-1} [74–76]. The intruding graphene layer can be adjusted by changing its Fermi energy level (Ef) through various significant means such as modifying gating voltage [77], substrate effect [78], external doping [79], and optical doping [80].

Graphene possesses a distinctive two-dimensional (2D) lattice structure comprising of a single layer of carbon atoms arranged in a hexagonal pattern [81], as depicted in Fig. 3. Due to its remarkable optical, electrical, and mechanical characteristics, graphene has become a subject of immense scientific and technological
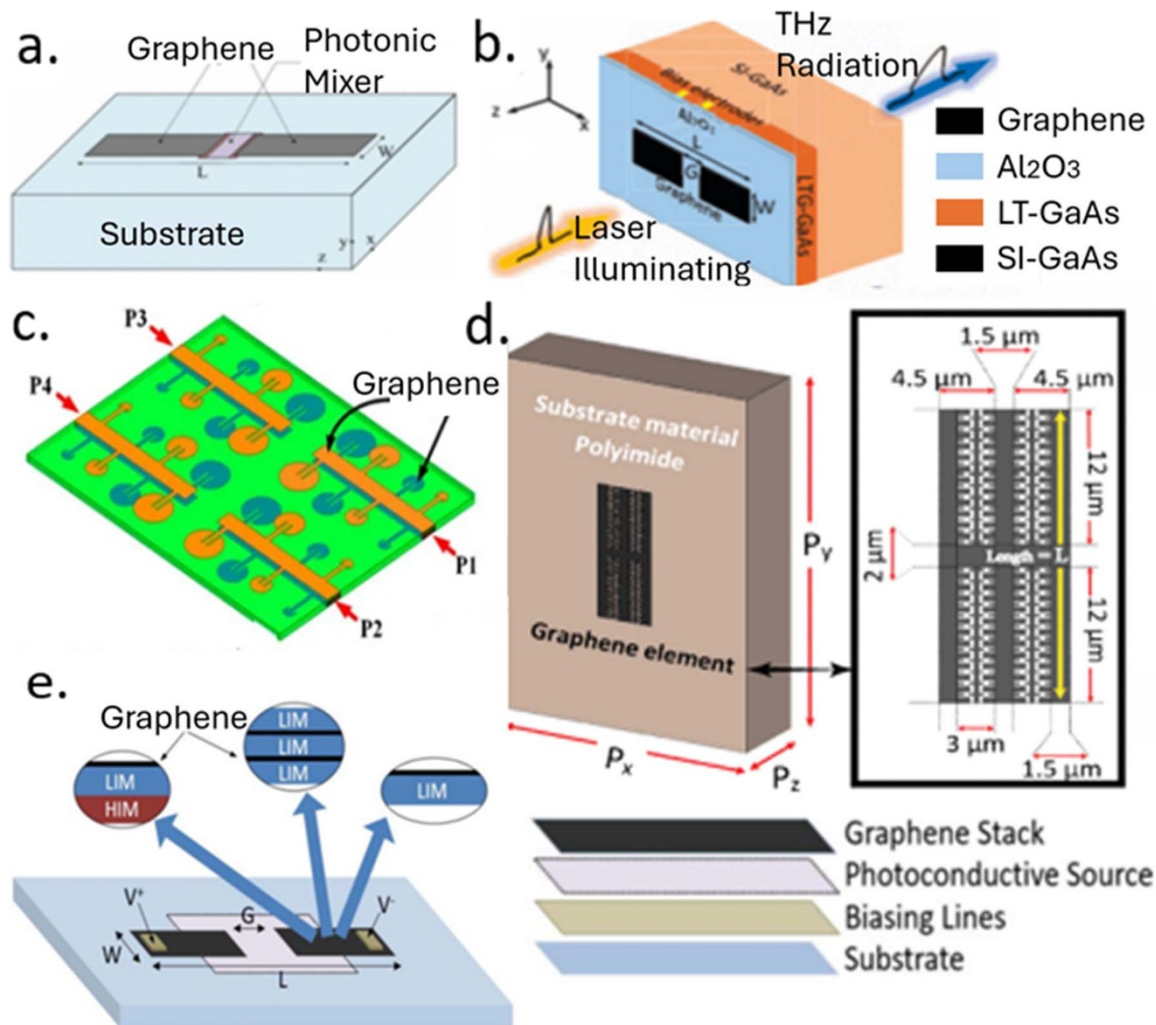
Figure 4. (a) A dipole PCA consists of two graphene strips placed on a substrate and integrated with a photo mixer at the antenna gap [99]. (b) A graphene-based PCA with superstrate combined with LT-GaAs and SI-GaAs [100]. (c) The schematic view of a graphene-based circular-patched Yagi-like THz MIMO antenna design [101]. (d) The schematic representation of the unit cell of a graphene-based THz sensor, while the design is a THz metasurface composed of a plurality of groups of the unit, showing a high sensitivity to THz waves on a broadband (0.2–6 THz) [102]. (e) A diagram illustrating a dipole PCA made of graphene with dimensions W × L, featuring a gap of length G and powered by a laser source. The electrodes may vary in structure, with different graphene-based stacks offering their unique benefits [103].

interest for manipulating its properties [82]. To investigate the electromagnetic properties of graphene, initial efforts focus on utilizing Maxwell's equations to model the electromagnetic waves propagating along the surface of graphene [83].

However, in some cases, Maxwell's equations lack analytical methods, so that the use of numerical methods is crucial in comprehending the behavior of guided waves as well as scattering phenomena in graphene [84]. The most used methods to analyze this problem include the finite-different time domain (FDTD) method [85–90], finite-element method [91, 92], and method of moments [93, 94]. The graphene model in theoretical electromagnetism study and antenna design can be simulated using various commercial simulation software, such as CST, COMSOL, HFSS, and FDTD solutions [84, 95]. Besides, several published PCA designs and simulations based on graphene are exhibited in Fig. 4.

The advantage of graphene-based PCA to generate THz waves lies in graphene's excellent carrier dynamics. After being excited by the light field, due to the ultra-fast carrier relaxation and relatively slow electron-hole recombination, the number of graphene

particles will be reversed near the Dirac point, resulting in the real part of the conductance oscillating in the THz range [96, 97]. Based on this, Dubinov designed a graphene heterojunction THz emitter containing a Fabri–Perot resonator [98]. In this design, graphene generates photoelectrons and holes under laser excitation. When a substantial quantity of electrons and holes are present in the conduction and valence bands, they generate THz radiation via the light-sound cascade phenomenon. The surface plasmons (SPs) have a comparatively low velocity, which results in a relatively high absorption coefficient, also known as SP gain. Consequently, it is significantly superior to conventional PCA with dielectric structures [98].

G. Hanson researched and proposed a conductivity model for graphene at THz frequencies [104]. Using the expression resulting from the Kubo formula [105], a conductivity equation is expressed as

$$\sigma(\omega) = \frac{2e^2}{\pi\hbar}\frac{k_B T}{\hbar}\ln\left[2\cosh\left(\frac{E_{F\gamma}}{2k_B T}\right)\right]\frac{i}{\omega + i_\tau^{-1}} \tag{5}$$
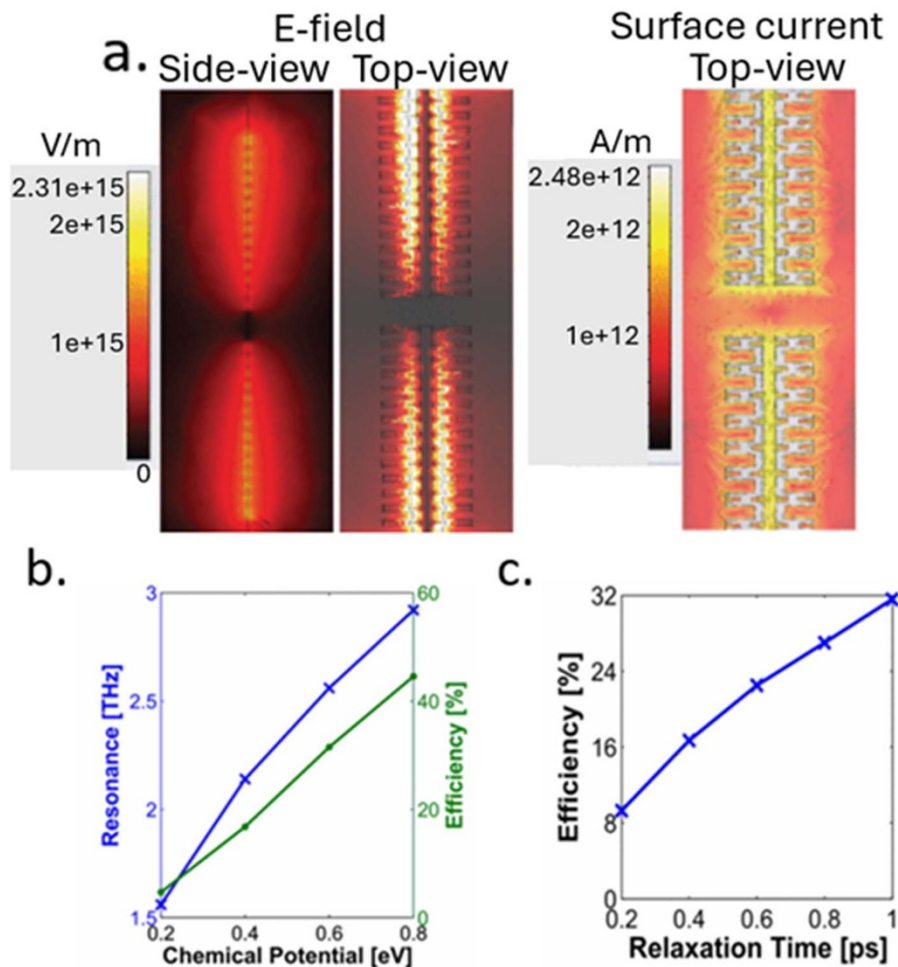
Figure 5. (a) *E*-field distribution and surface current of a unit cell of the graphene-based metasurface used in THz sensing [102]. (b) The resonance properties of the proposed graphene-based dipole PCA vary with the chemical potential EF [103]. (c) Efficiency enhancement depending on the relaxation time τ [103].

In this formula, three constants $\hbar$, e, and k_B represent the reduced Planck constant, the charge of one single electron, and the Boltzmann constant. Three variables T, E_F, and τ represent temperature, the chemical potential, and the relaxation time of the graphene layer. It indicates better performance with higher chemical potential variation ΔE_F. Meanwhile, high-quality graphene sheets display extended relaxation times, which increases their electrical conductivity and results in better antenna performance. From this, a THz metasurface sensor is proposed in [102], and a THz dipole is designed and simulated by Abadal with a graphene radiating element [103]. Figure 5(a) shows the high E-field distribution and surface current for the graphene element in Fig. 4(d). The results of [102] are illustrated in Fig. 5(b) and (c), demonstrating that the graphene-based THz PCA in Fig. 4(e) has improved both efficiency and gain, especially the former. In Fig. 5(b), the growth of chemical potential enhances the PCA performance, as the efficiency and gain increase by 52% and 0.46 dB, respectively, for E_F and τ are 0.8 eV and 1 ps. On the contrary, Fig. 5(c) demonstrates the resonant behavior being stronger as the relaxation time increases while the resonant frequency maintains. In this simulation, $E_F = 0.6$ eV and τ is variable. The efficiency and gain increased by 32% and 2.34 dB at $\tau = 1$ ps. In research of [106], a three-dimensional (3D) graphene-based photodetector exhibits a high specific detectivity of 1×10^{10} Jones and the response rate reaches 3.1 A/W under a excitation laser of 980 nm. Ref. [107] also uses graphene-based structure to significantly boost the coherent THz

detection among nonbiased THz emitters under room temperature. Ref. [108] illustrates PCAs using nanometer scale plasmonic structures based on graphene is capable of remarkable increase in responsibility (several orders of magnitude). The design in [109] achieves a noise equivalent power of less than 300 pW/$\sqrt{\text{Hz}}$.

Given these, graphene is playing and will continue to play a fundamental role in the future research of THz PCA on account of its unique features exhibited in the THz band. Current methods used in graphene materials in industrial fields are the solid phase method, vapor phase method, and liquid phase method [110]. However, achieving high-quality graphene monolayers is a significant hurdle in the research of graphene-based THz PCA. Unless corresponding industrial technology in graphene production is improved, otherwise the cost will be the reduction of radiation effects.

Geometrical configurations

In current PCA designs, a convenient and cheap way to enhance the THz output efficiency and power is to apply silicon lens in PCA designs [20, 21], and photonic crystals [36].

Silicon hyperhemispherical lens

During the optical-to-THz conversion process, the resulting THz waves experience significant diffraction at the interface between
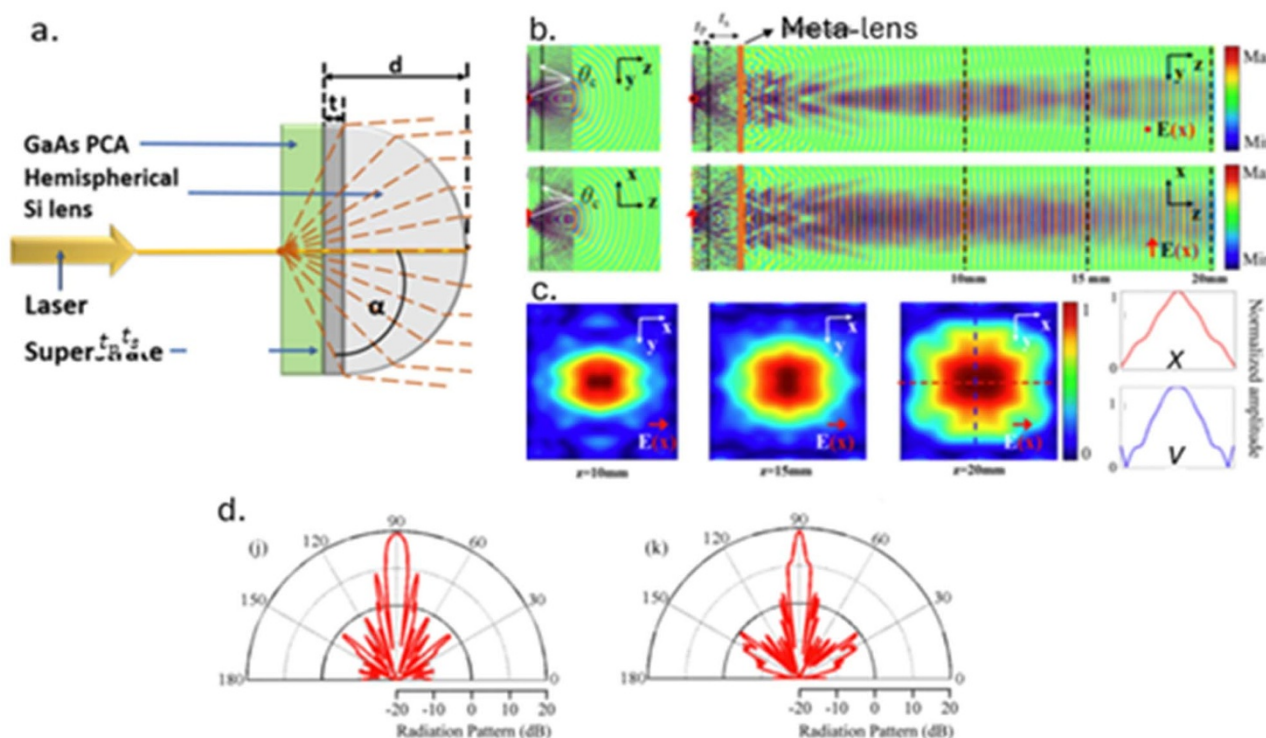
Figure 6. (a) PCA based on a hyperhemispherical lens excited by a laser source and the geometric dimension of lens design. (b) The simulation results of *E*-field distribution of a point current dipole PCA in both *y–z* plane and *x–z* plane. The *E*-field distributions along the *x*-axis at 1 THz are emitting through the meta-lens in the *y–z* plane and the *x–z* plane. (c) The simulation of cross-section amplitude distribution in the *x–y* plane when *z* = 10, 15, and 20 mm. (d) 1D far-field radiation pattern of the meta-lens on both the *y–z* plane and the *x–z* plane [20].

the substrate and the air. For most PCAs, GaAs is the material of substrates, which has a refractive index of $n \sim 3.4$ at THz frequencies. To increase the intensity of emitted THz waves, a hemispherical lens with a similar refractive index to GaAs can be used. Thus, with $n \sim 3.42$, silicon is the ideal material for the lens [111]. With the refractive index, the boundary angle α at which total reflection occurs can be computed as approximately 17.1° using arcsin (n^{-1}), and the solid angle Ω that describes the emitted THz waves is [112]

$$\Omega = 4\pi \sin^2 \frac{\alpha}{2} = 2\pi\left(1 - \cos\alpha\right) = 2\pi\left(1 - \sqrt{\frac{n^2-1}{n^2}}\right) \quad (6)$$

where α is the escape cone angle. The hyperhemispherical silicon lens helps increase the escape cone α due to its same refractive index [113]. To reduce the divergence in the air, the lens is supposed to be hyperhemispherical, with a certain distance d between the lens tip and the emitter [114]. As shown in Fig. 6(a), with the distance $d = R\left(1 + \frac{1}{n}\right)$, where n is considered as 3.4, it can be elicited as $d = 1.29\,R$ [112]. In these two equations, R represents the radius of the hemisphere.

Furthermore, in the research of [113] and [115], the theoretical analysis of a hyperhemispherical Si lens is proposed. Garufo et al. [21] proposed a PCA with silicon lens design in 2018 and the simulations show that the hyperhemispherical Si lens increased the radiation power by hundreds of μW within 0.1 and 1.5 THz. Zhu and Ziolkowski [116] mentions several PCA designs, which discuss the performance with hyperhemispherical Si lens providing theoretical research and experimental results support, mentioning that the efficiency and gain of these PCAs have all been improved to

over 80% and 13 dB. Research of [117] indicates that such Si hyperhemispherical lens also provides optimized performance of THz photodetectors by increasing resonant frequency in THz range.

Hyperhemispherical Si lenses are currently one of the simplest ways that are used in THz PCA efficiency and gain enhancement. There is still more improvement in lens designs. The research of [20] demonstrates the radiation of a PCA with Si meta-lens, as depicted in Fig. 6(b–d), establishing that the PCA exhibits extremely high transmittance and almost parallel collimation THz radiation in the THz band. Such approaches are of significant prospect for THz PCA and even spectroscopy.

Plasmonic nanostructures
With the development of nanotechnology, it is possible to apply nanostructures to the design of antennas. Currently, typical nanostructures have been applied to the design of THz PCA and have proved to be effective means to improve the efficiency of THz signal generation such as plasmonic structures and optical nanocavities, which lead to a higher level of interaction between the photoconductive semiconductor and the optically pumped beam [118].

To begin with, the plasmonic effect is the interaction of free electrons in metal nanoparticles with the incident electromagnetic field. This phenomenon is influenced by various factors such as the shape, size, spacing, and dielectric constant of the metal structure, as well as the material involved [119]. The interaction of metal nanoparticles with electromagnetic fields results in surface plasmon resonance, which generates a stronger local electric field [120]. The interaction between two plasmonic objects can squeeze the field and concentrate the local field when they are close enough to each other [33].
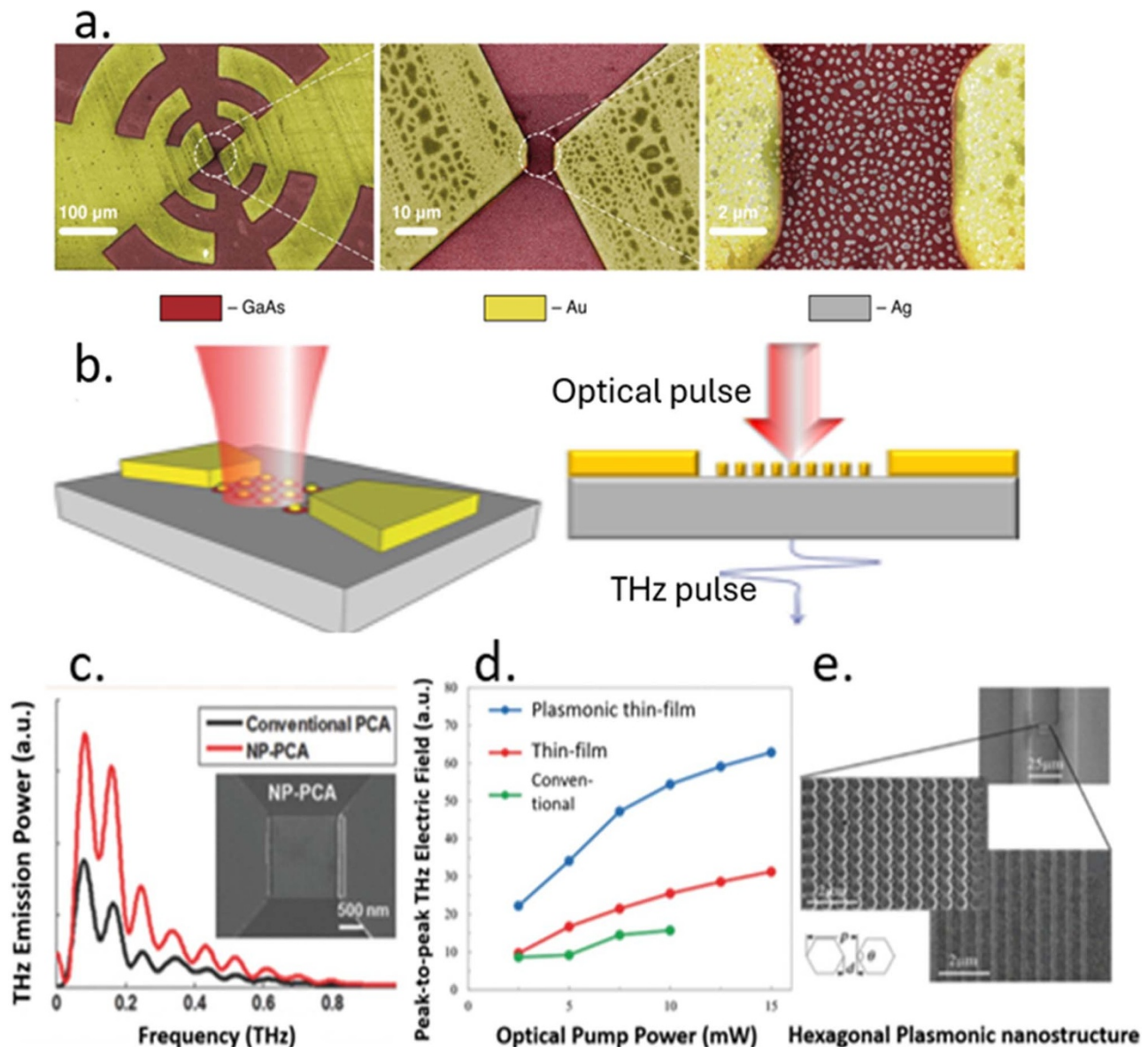
Figure 7. (a) Plasmonic concentrators (also known as quantum dots, or QD) that applied at the PCA gap [132]. (b) The demonstration of a PCA with plasmonic concentrators design [118]. (c) Comparison of measured THz emission power with conventional design and plasmonic concentrators design. (d) Comparison of radiation results of PCA with hexagonal nanostructure, plasmonic light concentrators, and conventional design. (e) SEM of the hexagonal plasmonic nanostructure [31].

Notably, the metal plasmonic nano designs include concentrators at the gap, and contact electrodes, both to enhance the optical-to-THz conversion efficiency of THz PCA [121]. The configuration of the plasmonic concentrators is intended to generate surface plasmon waves when illuminated by optical pumps. Surface plasmons refer to the coherent oscillations of electrons that arise at the interface of a metal and a dielectric medium. Upon coupling with an incident electromagnetic wave, the resultant surface plasmons have the ability to propagate along the dielectric interface [122]. To enable the coupling of surface plasmons with electromagnetic waves, certain mechanisms need to be put in place. It is necessary to ensure that the parallel wave vectors of both match, which can be determined from both the metal and the dielectric permittivity values [123]. By matching the electromagnetic waves and surface plasmon wave vectors of the metal surface, the graphic patterning of the metal surface can promote the excitation of the

surface plasmon waves [124]. The capacity to stimulate surface plasmon waves offers a range of exceptional possibilities for directing and controlling electromagnetic waves [118]. Such plasmonic nanostructures facilitate a high concentration of laser in the near field while opening the way to both THz transmitting PCA and receiving PCA with higher efficiency [125–131].

According to the above study on the plasmonic concentrators, [133–137] have verified that such concentrators improve the optical-to-THz efficiency of THz PCA. The concentrators confine the stimulated surface plasmon waves very closely to the interface between the metal and the photoconductor, thus the laser absorption of the photoconductive substrate near the polymerized structure is significantly enhanced; therefore, the generation of photo carriers in the substrate region is enhanced. Ultimately, the radiation power level increases as the number of photo carriers reaching the antenna electrode increases.
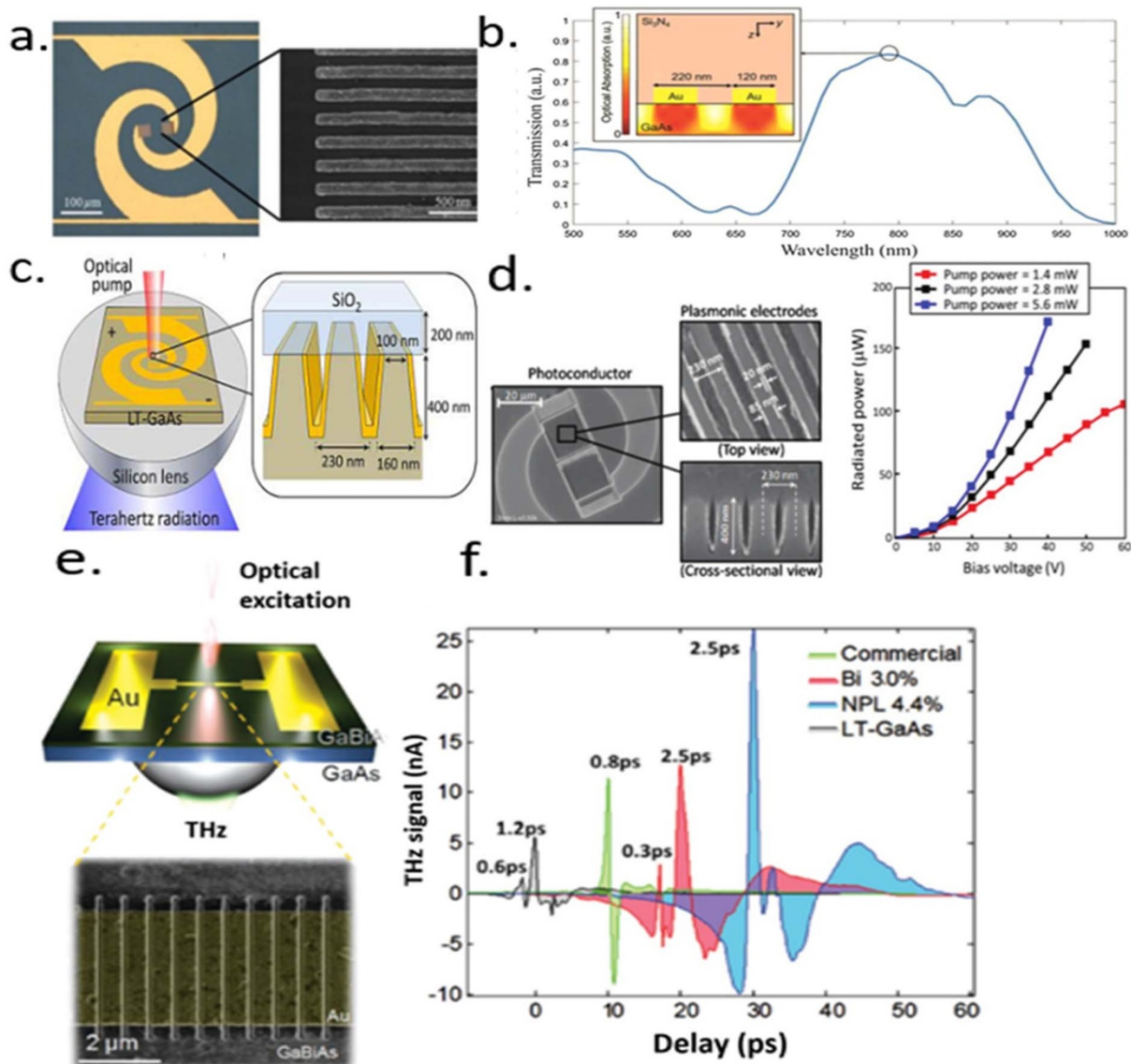
Figure 8. (a) and (b) A log-spiral PCA design with plasmonic contact electrodes and the figure of the optical transmission performance [41]. (c) and (d) The demonstration and SEM of a 3D plasmonic gratings design for PCA contact electrodes and the measured radiation power comparison with different excite power of 1.4, 2.8, and 5.8 mW [24]. (e) The implementation and SEM figure of an unincorporated plasmonic grating at the PCA gap. (f) The comparison of THz signal amplitude due to different structures, showing a more than 2 times increase with this structure [121].

The research of [138, 139] and [140] provides the comparison between conventional PCA and novel PCA with plasmonic nano concentrators, all based on semi-insulating (SI) GaAs substrate and excited by 800 nm wavelength optical pump, shown in Fig. 7. As a result, an approximately 100% increment over the 0.1–1.1 THz range is implemented to the radiation power in [138]. The theoretical principle of the absorbed optical power P by the substrate in volume V can be explained by [121]:

$$P = \frac{1}{2} \int^{\sigma} \delta^2 |E_0|^2 dV \tag{7}$$

As $\delta = \frac{|E|}{|E_0|}$, σ is a medium conductivity, with E increased, there is also an increase on the concentration of nonequilibrium charge carriers near the electrodes. Therefore, the optical-to-THz efficiency is enhanced. In another study, a similar nanostructure was applied to PCA with SI-GaAs substrate. In contrast to the basic

plasmonic concentrators, a hexagonal plasmonic structure is proposed [139, 140], and including the conventional optical antenna, all three PCA designs are measured and compared. Hexagonal nanostructures were shown to provide stronger current density localization. The scanning electron microscope (SEM) images of all three PCAs are shown in Fig. 7(c–e). Consequently, the resulting THz field of the hexagonal plasmonic nanostructure is over three times enhanced compared to the PCA with normal plasmonic concentrators, and five times enhanced compared to the conventional PCA.

In more recent studies, another plasmonic nanostructure has been proposed, which applies a novel geometric design to the electrodes, also known as contact fingers [141–143]. Similar to the plasmonic optical concentrator, the plasmonic contact electrode can excite the surface plasmon waves and tightly confine them to the metal–photoconductor interface, thereby increasing the laser absorption in the active region of the photoconductor near the
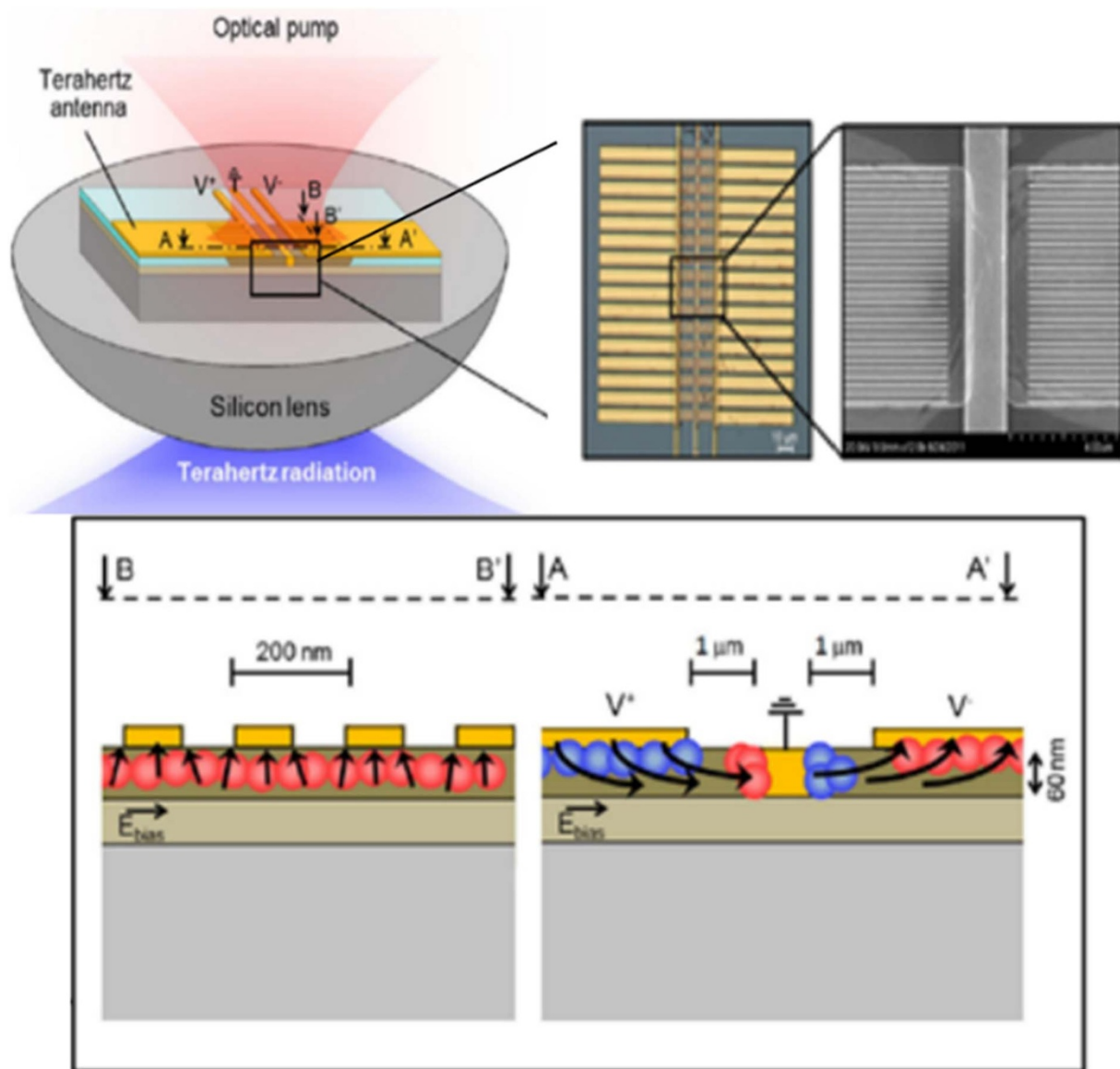
Figure 9. An implementation of plasmonic contact electrode design and the SEM figure [120].

contact electrodes. Another advantage of using such a method is that they are connected directly to the THz PCA, which shortens the transmission path of the photo carriers to the electrodes [144]. Thus, the utilization of plasmonic contact electrodes not only leads to an increase in the efficiency of converting optical energy to THz radiation but also significantly shortens the transport time of photo carriers transported to the PCA when compared to light concentrators. A logarithmic spiral PCA with plasmonic contact electrodes is depicted in Fig. 8(a), along with the optical transmission spectrum through the grating and its corresponding transmission performance, as shown in Fig. 8(b) [41]. With such a structure, a 1.9 mW THz radiation power increase is obtained at the 0.1–2 THz range [145].

Moreover, Fig. 8(c) and (d) shows a 3D plasmonic gratings design for PCA contact electrodes [24]. This research shows a record-high 7.5% conversion efficiency from optical power to THz radiation power. Another similar study proves a 40-fold stronger output photocurrent in response to an incident THz pulse compared with conventional design. All these PCAs are excited by an 800 nm laser [124]. Meanwhile [146] and [147] use unincorporated plasmonic grating to the PCA gap to enhance the generation of THz pulses. Such metal strips reduce the lifetime of electrons in semiconductors. The PCAs are based on GaAsBi semiconductor substrate, whose carrier lifetime is shorter than that of LT-GaAs substrate [147], and the amplitude of the THz signal can be increased by more than 2 times by using this structure, as shown in Figs. 8(e) and (f). However, compared with other methods, this design has a lower optical-to-THz conversion enhancement due to its large capacitance [146].

Figure 9 [120] shows another implementation of plasmonic contact electrode design, and the comparison of THz emission power with different optical excite power is shown in Fig. 10(a). The end of the fingers is connected in this PCA, which significantly reduces the path of photo carriers. However, a disadvantage of this design is proved by [120]: The efficiency of these structures is restricted to 50%, due to only half of the nonequilibrium
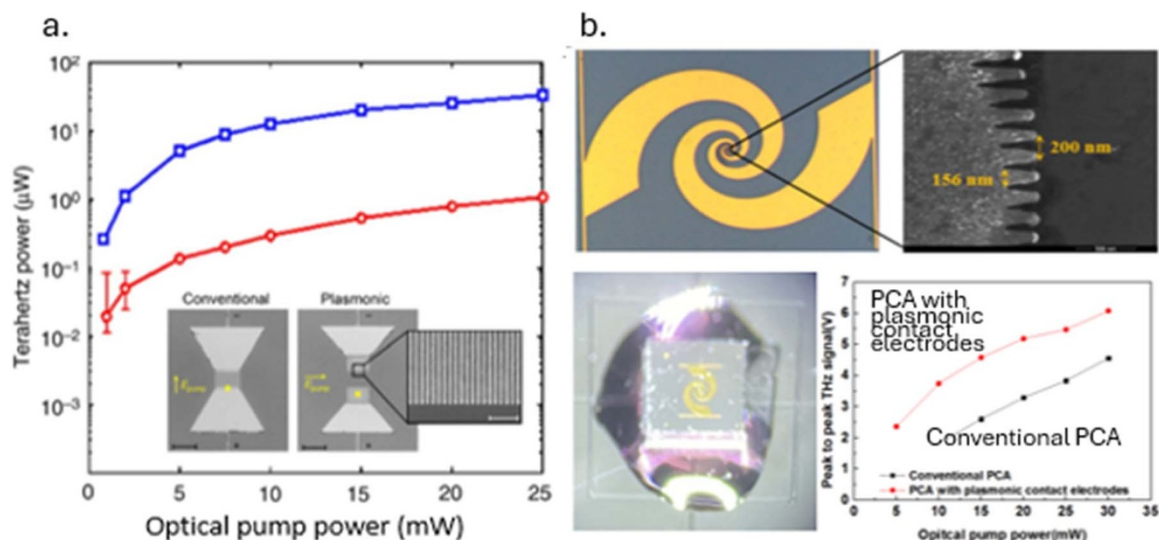
Figure 10. (a) The THz power comparison with corresponding optical pump power [121]. (b) A PCA featuring toothed plasmonic contact electrodes has been developed and is presented along with a photograph of the fabricated antenna under a microscope. A comparison between the proposed PCA and a conventional PCA is also included [148].

electrons and holes being able to reach the internal electrodes within a picosecond timeframe.

Altogether, with the advancement of nanomanufacturing technology, the integration of plasmonic nanostructures is poised to enable substantial improvements in the performance of the forthcoming generation of high-performance, cost-effective PCAs.

Photonic crystals

It has been investigated that surface plasmon resonance can improve the local electrical field. In the design of THz PCA, there is another efficiency improvement method based on this theory. The photonic crystal structure can be used in the design of the substrate when the substrate is thick [36]. Based on this, a THz PCA design with a 2D hexagonal lattice of air holes drilled into the substrate is proposed and investigated in [36], shown in Fig. 11(a). This research proves that this structure can improve both efficiency and directivity. The hexagonal lattice of the proposed structure contains a defect core region that is comparable to the solid photonic crystal waveguide described in [149]. This region coincides with the excitation gap of the PCA. By incorporating this defect core region, the effective dielectric constant of the substrate is reduced, which results in a guiding mechanism along the defect axis. Consequently, the effective thickness of the substrate is also decreased, leading to reduced power leakage [36].

As shown in Fig. 11(c) and (d), with the appropriate photonic crystal substrate design, the radiation power is primarily positioned around the defect and directed along the axis of the defect. As a result, the radiation in transverse directions decreases. Therefore, the two major advantages of such designs are summarized as follows. Firstly, the radiated power is mainly oriented along the axis of the defect, so that the main lobe of the radiation pattern is oriented towards the Z-axis within the entire operating bandwidth. This will make the directivity significantly improved. Besides, the photonic crystal structure can reduce the capture power in the substrate, thus improving the radiation efficiency [34–36]. This structure provides an average radiation efficiency enhancement of 81%, and an average directivity enhancement of 10.9 dBi over 0.65–1.45 THz, shown in Fig. 11(b).

In a comparative study, a photonic crystal substrate is used in a PCA array design, which improves the radiation efficiency to 96% as that of the conventional contrast design is less than 55%, both in the 0.7–1.4 THz range. The directivity enhancement of this study is over 5 dBi [150].

Therefore, it is suggested that the THz conductivity and the radiation characteristics of PCA can be improved by using this structure in future research. The proposed substrate is an effective and low-cost method for obtaining high directivity and suitable radiation patterns of PCA arrays, as well as reducing the necessity of using hyperhemispherical silicon lens.

Future prospects

The advancement of photoconductive antennas (PCAs) has been driven by developments in materials, innovative geometries, and femtosecond laser applications. This review closely examines the first two factors, emphasizing the challenge of enhancing optical-to-THz conversion efficiency for future work. Achieving this improvement depends on multiple factors, particularly the choice of photoconductive materials and electrode configurations, which are analyzed in this study.

Although material research has progressed significantly, current fabrication techniques still fall short of fully realizing PCA capabilities. Further exploration into material physics promises potential breakthroughs, introducing advanced photoconductive materials to the field. While complex methods like photonic crystal and plasmonic nanostructures can improve THz radiation, they contradict the PCA's core principle of design simplicity. Hence, a key research focus is developing novel, simplified structures that enhance THz radiation without compromising PCA's intrinsic simplicity. The future material research will include the use of topological insulators such as bismuth selenide, and novel nanoparticles such as graphene quantum dots and molybdenum disulfide.

Recent years have seen notable progress in radiation enhancement techniques, such as metasurfaces, which are well-optimized and show potential for extending their operational range to THz frequencies—utilizing both PCA and metasurfaces in future THz communication applications is a promising research direction.
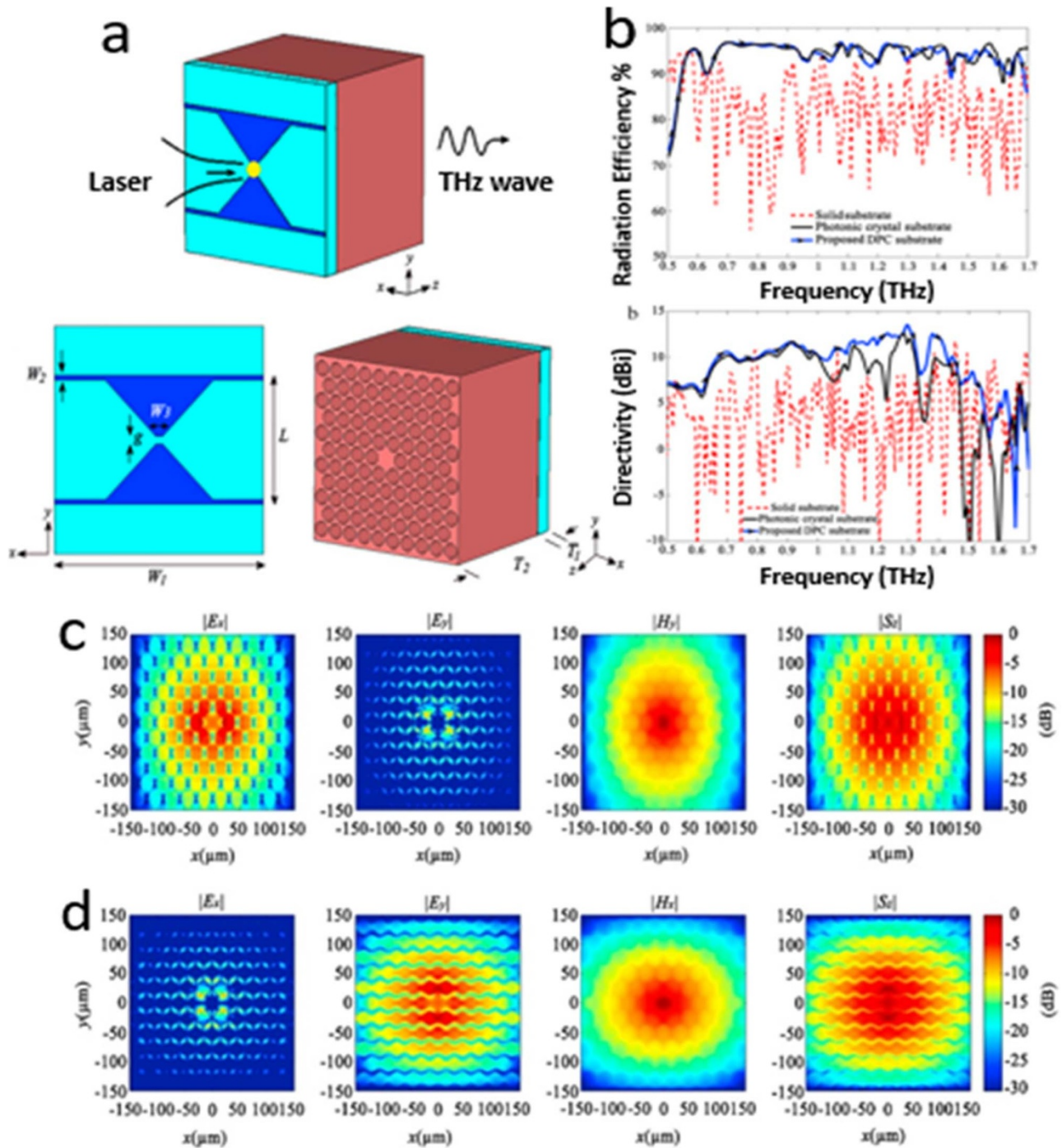
Figure 11. (a) The demonstration of a bowtie PCA with photonic crystal substrate structure. (b) The comparison of radiation efficiency and directivity respect to frequency [36]. (c) and (d) The radiation power magnitude of transverse electric and magnetic modal fields (|Ex|, |Ey|, |Hx|, and |Hy|) as well as longitudinal power flow (|Sz|) for the two modes of photonic crystal structure in *xy*-plane in the research of [36].

Ultimately, advancing optical-to-THz conversion efficiency and THz wave generation could open new avenues for PCAs, offering transformative contributions to the field and reshaping future communication technologies.

Conclusion

This review examines various approaches to enhancing the efficiency of THz PCAs, focusing on material selection and structural design. For instance, advancements in photoconductive and 2D materials significantly improve optical-to-THz conversion efficiency. Additionally, innovative geometric designs in PCA gaps, electrode configurations, and substrates boost radiation output. All studies presented in this review are based on THz transmission PCAs, generating THz pulses excited by laser sources. In summary, THz antennas offer a landscape rich with opportunities and challenges, where even minor improvements in power generation and system design could

unlock new directions for advancing future communication systems.

References

1. **Lee Y** (2008) *Principles of Terahertz Science and Technology*, 1st Edn., New York: NY: Springer.

2. **Tabata H** (2015) Application of terahertz wave technology in the biomedical field. *IEEE Transactions on Terahertz Science and Technology* **5**(6), 1146–1153.

3. **Zeitler JA, Taday PF, Newnham DA, Pepper M, Gordon KC and Rades T** (2010) Terahertz pulsed spectroscopy and imaging in the pharmaceutical setting - a review. *Journal of Pharmacy and Pharmacology* **59**(2), 209–223.

4. **Pozniak H** (2021) T-ray imaging gets under the skin: A method for analysing the structure of skin using a type of radiation known as T-rays could help improve the diagnosis and treatment of skin conditions. *Engineering & Technology* **16**(2), 48–49. https://doi.org/10.1049/et.2021.0209

5. **Chen H, Han J, Ma S, Li X, Qiu T and Chen X** (2022) Clinical diagnosis of gastric cancer by high-sensitivity THz fiber-based fast-scanning near-field imaging. *Cancers (Basel)* **14**(16), 3932. https://doi.org/10.3390/cancers14163932

6. **King MD, Buchanan WD and Korter TM** (2010) Understanding the terahertz spectra of crystalline pharmaceuticals: Terahertz spectroscopy and solid-state density functional theory study of (S)-(+)-ibuprofen and (RS)-ibuprofen. *Journal of Pharmaceutical Sciences* **100**, 1116–1129. https://doi.org/10.1002/jps.22339

7. **Ho L, Pepper M and Taday P** (2008) Terahertz spectroscopy: Signatures and fingerprints. *Nature Photonics* **2**, 541–543. https://doi.org/10.1038/nphoton.2008.174

8. **Tonouchi M** (2007) Cutting-edge terahertz technology. *Nature Photonics* **1**(2), 97–105. https://doi.org/10.1038/nphoton.2007.3

9. **Chen Y, Qin F, Liu L, Zhao Z, Li P, Sun Y, Liu W and Wang Y** (2025) 0.4 THz broadband terahertz noise source based on photoconductive antennas. *Photonics* **12**, 252. https://doi.org/10.3390/photonics12030252

10. **Ponomarev DS, Lavrukhin DV, Glinskiy IA, Yachmenev AE, Zenchenko NV, Khabibullin RA, Goncharov YG, Otsuji T and Zaytsev KI** (2023) Enhanced THz radiation through a thick plasmonic electrode grating photoconductive antenna with tight photocarrier confinement. *Optics Letters* **48**, 1220–1223. https://doi.org/10.1364/OL.486431

11. **Gorodetsky A Lavrukhin DV, Ponomarev DS, Smirnov SV, Yadav A, Khabibullin RA and Rafailov EU** (2023) Enhanced THz generation from interdigitated quantum dot based photoconductive antenna operating in a quasi-ballistic regime. *IEEE Journal of Selected Topics in Quantum Electronics* **29**(5), 1–5. Terahertz Photonics https://doi.org/10.1109/JSTQE.2023.3271830

12. **Ghorbani S, Bashipour M and Kolahdouz M** (2019) Improving unbiased terahertz photoconductive antenna based on dissimilar Schottky barriers using plasmonic mode excitation. *Optik* **194**, 162975. https://doi.org/10.1016/j.ijleo.2019.162975

13. **Pavlidis D** (2021) *Fundamentals of Terahertz Devices and Applications*. Florida: Wiley.

14. **Bacon DR, Madeo J and Dani KM** (2021) Photoconductive emitters for pulsed terahertz generation. *Journal of Optics* **23**(6), 064001. https://doi.org/10.1088/2040-8986/abf6ba

15. **He Y, Chen Y, Zhang L, Wong S-W and Chen Z** (2020) An overview of terahertz antennas. *China Communications* **17**(7), 124–165. https://doi.org/10.23919/J.CC.2020.07.011

16. **Isgandarov E, Ropagnol X, Singh M and Ozaki T** (2021) Intense terahertz generation from photoconductive antennas. *Frontiers of Optoelectronics* **14**, 64–93. https://doi.org/10.1007/s12200-020-1081-4

17. **Arora N** (2022) Prospective materials for photoconductiveantennas for terahertz generation. *Journal of Innovation and Social Science Research* **9**(89), 155–158.

18. **Kar S, Lake J, Adeyemo SO, Santra TS and Joyce HJ** (2022) The physics of terahertz negative photoconductivity in low-dimensional materials. *Materials Today Physics* **23**, 100631. https://doi.org/10.1016/j.mtphys.2022.100631

19. **Burford NM and El-Shenawee MO** (2017) Review of Terahertz Photoconductive Antenna Technology. *Optical Engineering* **56**(1), 1–20.

20. **Yu Q, Gu J, Yang Q, Zhang Y, Li Y, Tian Z, Ouyang C, Han J, O'Hara JF and Zhang W** (2017) All-dielectric meta-lens designed for photoconductive terahertz antennas. *All-Dielectric Meta-lens Designed for Photoconductive Terahertz Antennas* **9**(4), 1–9.

21. **Garufo A, Sberna P, Carluccio G, Bueno J, Freeman J, Llombart N, Linfield EH, Davies AG and Neto A** (2018) Leaky lens antenna as optically pumped pulsed THz emitter In 2018 43rd International Conference on Infrared, Millimeter, and Terahertz Waves, Nagoya, Japan.

22. **Catrysse PB, Veronis G, Shin H, Shen J-T and Fan S** (2006) Guided modes supported by plasmonic films with a periodic arrangement of subwavelength slits. *Applied Physics Letters* **88**(3), 031101. https://doi.org/10.1063/1.2164905

23. **Hsieh B-Y and Jarrahi M** (2011) Analysis of periodic metallic nano-slits for efficient interaction of terahertz and optical waves at nano-scale dimensions. *Journal of Applied Physics* **109**(8), 084326. https://doi.org/10.1063/1.3567909

24. **Yang S-H and Jarrahi M** (2013) Enhanced light–matter interaction at nanoscale by utilizing high-aspect-ratio metallic gratings. *Optics Letters* **38**(18), 3677–3679. https://doi.org/10.1364/OL.38.003677

25. **Moradiannejad F** (2021) Improvement of terahertz photoconductive antennas array using crossfingers structure. *Journal of Computational Electronics* **20**, 922–927. https://doi.org/10.1007/s10825-021-01661-3

26. **Dreyhaupt A, Winnerl S, Dekorsy T and Helm M** (2004) High-intensity terahertz radiation from a microstructured large-area photoconductor. *Applied Physics Letters* **86**(12), 121114.

27. **Beck M, Schafer H, Klatt G, Demsar J, Winnerl S, Helm M and Dekorsy T** (2010) Impulsive terahertz radiation with high electric fields from an amplifier-driven large-area photoconductive antenna. *Optics Express* **18**(9), 9251. https://doi.org/10.1364/OE.18.009251

28. **Yardimci NT, Yang SH, Berry CW and Jarrahi M** (2015) High power terahertz generation using large area plasmonic photoconductive emitters. *IEEE Transactions on Terahertz Science and Technology* **5**(2), 223–229. https://doi.org/10.1109/TTHZ.2015.2395417

29. **Yardimci NT, Salas R, Krivoy EM, Nair HP, Bank SR and Jarrahi M** (2015) Impact of substrate characteristics on performance of large area plasmonic photoconductive emitters. *Optics Express* **23**(25), 32035–32043. https://doi.org/10.1364/OE.23.032035

30. **Turan D, Corzo-Garcia SC, Yardimci NT, Castro-Camus E and Jarrahi M** (2017) Impact of the metal adhesion layer on the radiation power of plasmonic photoconductive terahertz sources. *Journal of Infrared, Millimeter, and Terahertz Waves* **38**, 1448–1456. https://doi.org/10.1007/s10762-017-0431-9

31. **Yardimci NT and Jarrahi M** (2017) High sensitivity terahertz detection through large-area plasmonic nano-antenna arrays. *Scientific Reports* **7**, 42667. https://doi.org/10.1038/srep42667

32. **Berry CW, Hashemi MR and Jarrahi M** "Plasmonic photoconductive terahertz emitters based on logarithmic spiral antenna arrays," in Proc. 2013

38th InternationalConference on Infrared, Millimeter, and Terahertz Waves (IRMMW-THz), Mainz, 2013.

33. **Berry CW, Wang N, Hashemi MR, Unlu M and Jarrahi M** (2013) Significant performance enhancement in photoconductive terahertz optoelectronics by incorporating plasminic contact electrodes. *Nature Communications* **4**(3), 1622–1632. https://doi.org/10.1038/ncomms2638

34. **Garufo A, Carluccio G, Llombart N and Neto A** (2018) Norton equivalent circuit for pulsed photoconductive antennas part I: Theoretical model. *IEEE Transactions on Antennas and Propagation* **66**(4), 1635–1645. https://doi.org/10.1109/TAP.2018.2800524

35. **Garufo A, Carluccio G, Freeman JR, Bacon DR, Llombart N, Linfield EH, Davies AG and Neto A** (2018) Norton equivalent circuit for pulsed photoconductive antennas. Part II: Experimental validation. *IEEE Transactions on Antennas and Propagation* **66**(4), 1646–1659. https://doi.org/10.1109/TAP.2018.2800704

36. **Rahmati E and Ahmadi-Boroujeni M** (2018) Improving the efficiency and directivity of THz photoconductive antennas by using a defective photonic crystal substrate. *Optics Communications* **412**, 74–79. https://doi.org/10.1016/j.optcom.2017.12.011

37. **Rafailov EU, Cataluna MA and Sibbett W** (2007) Mode-locked quantum-dot lasers. *Nature Photonics* **1**(7), 395–401. https://doi.org/10.1038/nphoton.2007.120

38. **Porte HP, Jepsen PU, Daghestani N, Rafailov EU and Turchinovich D** (2009) Ultrafast release and capture of carriers in InGaAs/GaAs quantum dots observed by time-resolved terahertz spectroscopy. *Applied Physics Letters* **94**, 262104. https://doi.org/10.1063/1.3158958

39. **Gorodetsky A, Bazieva N and Rafailov EU** (2019) Pump dependent carrier lifetimes in InAs/GaAs quantum dot photoconductive terahertz antenna structures. *Journal of Applied Physics* **125**(15), 151606. https://doi.org/10.1063/1.5083798

40. **Yeh K-L, Hoffmann MC, Hebling J and Nelson K** (2007) Generation of 10μJ ultrashort terahertz pulses by optical rectification. *Applied Physics Letters* **90**(17), 171121. https://doi.org/10.1063/1.2734374

41. **Alharbi A, Alshamrani N, Hussain H, Alhamdan M and Alfihed S** (2023) Two-dimensional materials for terahertz emission. *Trends in Terahertz Technology.* IntechOpen, Sept. 27, 2023. https://doi.org/10.5772/intechopen.110878

42. **Xie M and Lu G**, "Research on terahertz photoconductive antenna," in Proc. 2017 IEEE 5th International Symposium on Electromagnetic Compatibility (EMC-Beijing), Beijing, 2017.

43. **Cabello NI, De Los Reyes A, Sarmiento V, Ferrolino JP, Vistro VD, Vasquez JD, Bardolaza H, Kitahara H, Tani M, Salvador A and Somintac A** (2022) Terahertz emission enhancement of gallium-arsenide-based photoconductive antennas by silicon nanowire coating. *IEEE Transactions on Terahertz Science and Technology* **12**(1), 36–41. https://doi.org/10.1109/TTHZ.2021.3115726

44. **Li Y-T, Shi J-W, Huang C-Y, Chen N-W, Chen S-H, Chyi J-I and Pan C-L** (2008) Characterization of sub-THz photonic-transmitters based on GaAs–AlGaAs uni-traveling-carrier photodiodes and substrate-removed broadband antennas for impulse-radio communication. *IEEE Photonics Technology Letters* **20**(16), 1342–1344. https://doi.org/10.1109/LPT.2008.926855

45. **Sartorius B, Roehle H, Kunzel H, Bottcher J, Schlak M, Stanze D, Venghaus H and Schell M** (2008) All-fiber terahertz time-domain spectrometer operating at 1.5 um telecom wavelengths. *Optics Express* **16**(13), 9565–9570. https://doi.org/10.1364/OE.16.009565

46. **Ellrich F, Weinland T, Molter D, Jonuscheit J and Beigang R** (2011) Compact fibercoupled terahertz spectroscopy system pumped at 800 nm wavelength. *Review of Scientific Instruments* **82**(5). https://doi.org/10.1063/1.3587070

47. **Shaw JA** (2013) Radiometry and the friis transmission equation. *American Journal of Physics* **81**(1), 33–37. https://doi.org/10.1119/1.4755780

48. **Tamminen A, Makela S, Ala-Laurinaho J, Hakli J, Koivisto P, Rantakari P, Saily J, Luukanen A and Raisanen AV** (2013) Reflectarray design for 120-ghz radar application: Measurement results. *IEEE Transactions on Antennas and Propagation* **61**(10), 5036–5047. https://doi.org/10.1109/TAP.2013.2273256

49. **Auston DH, Cheung KP and Smith PR** (1984) Picosecond photoconducting Hertzian dipoles. *Applied Physics Letters* **45**, 284–286. https://doi.org/10.1063/1.95174

50. **Goldsmith PF** (1998) *Quasioptical Systems: Gaussian Beam Quasioptical Propogation and Applications*. Wiley-IEEE Press. New York: Chapman & Hall.

51. **Hou X, Wen L, Fengyue H, Zhuo R, Liu L, Wang H, Zhong Q, Pan D and Zhao J** (2024) Embedded high-quality ternary GaAs1−xSbx quantum dots in GaAs nanowires by molecular-beam epitaxy. *Journal of Semiconductors* **45**(8), 082101. https://doi.org/10.1088/1674-4926/24030038

52. **Karthikeyan S, Johnston SW, Gayakwad D, Mahapatra S, Bodnar RJ, Zhao J, Joshi R and Hudait MK** (2024) GeSn-on-GaAs with photoconductive carrier lifetime >400 ns: Role of substrate orientation and atomistic simulation. *Nanoscale* **16**(14), 7225–7236. https://doi.org/10.1039/D3NR05904A

53. **Chuang S -L.** (2009) *Physics of Photonic Devices*. Hoboken, New Jersey: John Wiley & Sons, p. 113.

54. **Chia JY, Zhang Y, Li K, Kusolthossakul W, Sathukarn A, Tantiwanichapan K, Rattanawan P, Jintamethasawat R, Thamrongsiripak N and Nuntawong N** (2022) Facile activation of a GaAs substrate with electron beam irradiation for THz photoconductive antenna. *Applied Physics Express* **15**(10), 107002. https://doi.org/10.35848/1882-0786/ac926d

55. **Chen W-C and Yang S-H** (2022) Thermal evaporated group IV Ge(Sn)-on-Si terahertz photoconductive antenna. *Optics Express* **30**(18), 31742–31751. https://doi.org/10.1364/OE.466108

56. **Smith FW, Le HQ, Diadiuk V, Hollis MA, Calawa AR, Gupta S, Frankel M, Dykaar DR, Mourou GA and Hsiang TY** (1989) Picosecond GaAs-based photoconductive optoelectronic detectors. *Applied Physics Letters* **54**(10), 890–892. https://doi.org/10.1063/1.100800

57. **Warren AC, Katzenellenbogen N, Grischkowsky D, Woodall JM, Melloch MR and Otsuka N** (1991) Subpicosecond, freely propagating electromagnetic pulse generation and detection using GaAs:As epilayers. *Applied Physics Letters* **58**(14), 1512–1514. https://doi.org/10.1063/1.105162

58. **Gupta S, Frankel MY, Valdmanis JA, Whitaker JF, Mourou GA, Smith FW and Calawa AR** (1991) Subpicosecond carrier lifetime in GaAs grown by molecular beam epitaxy at low temperatures. *Applied Physics Letters* **59**(25), 3276–3278. https://doi.org/10.1063/1.105729

59. **Kono S, Tani M, Gu P and Sakai K** (2000) Detection of up to 20 THz with a low-temperature-grown GaAs photoconductive antenna gated with 15 fs light pulses. *Applied Physics Letters* **77**(25), 4104–4106. https://doi.org/10.1063/1.1333403

60. **Nemec H, Pashkin A and Kuzel P** (2001) Carrier dynamics in low-temperature grown GaAs studied by terahertz emission spectroscopy. *Journal of Applied Physics* **90**(3), 1303–1306. https://doi.org/10.1063/1.1380414

61. **Kadow C, Jackson AW, Gossard AC, Bowers JE, Matsuura S and Blake GA** (2000) Self-assembled ErAs islands in GaAs for THz applications. *Physica E: Low-dimensional Systems and Nanostructures* **7**(1-2), 97–100. https://doi.org/10.1016/S1386-9477(99)00314-8

62. **Bjamason JE, Chan TL, Lee AW, Brown ER, Driscoll DC, Hanson M, Gossard AC and Muller RE** (2004) ErAs:GaAs photomixer with two-decade tunability and 12 μW peak output power. *Applied Physics Letter* **85**, 3983-3985.

63. **Liu T-A, Tani M, Nakajima M and Hangyo M** (2003) Ultrabroadband terahertz field detection by photoconductive antennas based on multi-energy arsenic-ion-implanted GaAs and semi-insulating GaAs. *Applied Physics Letters* **83**(7), 4664–4666. https://doi.org/10.1063/1.1630378

64. **Tani M, Matsuura S, Sajai K and Nakashima S-I** (1997) Emission characteristics of photoconductive antennas based on low-temperature-grown GaAs and semi-insulating GaAs. *Applied Optics* **36**(30), 7853–7859. https://doi.org/10.1364/AO.36.007853

65. **Beard MC, Turner GM and Schmuttenmaer CA** (2001) Subpicosecond carrier dynamics in low-temperature grown GaAs as measured by time-resolved terahertz spectroscopy. *Journal of Applied Physics* **90**(12), 5915–5923. https://doi.org/10.1063/1.1416140

66. **Jo SJ, Ihn S-G and Song J-I** (2005) Carrier dynamics of low-temperature-grown In0.53Ga0.47As on GaAs using an InGaAlAs metamorphic buffer. *Applied Physics Letter* **86**(11), 111903. https://doi.org/10.1063/1.1872207

67. **Stone MR, Naftaly M, Miles RE, Fletcher JR and Steenson DP** (2004) Electrical and radiation characteristics of semilarge photoconductive terahertz emitters. *IEEE Transactions on Microwave Theory and Techniques* **52**(10), 2420–2429. https://doi.org/10.1109/TMTT.2004.835980

68. **Takazato A, Kamakura M, Matsui T, Kitagawa J and Kadoya Y** (2007) Terahertz wave emission and detection using photoconductive antennas made on low-temperature-grown InGaAs with 1.56μm pulse excitation. *Applied Physics Letter* **91**(1), 011102. https://doi.org/10.1063/1.2754370

69. **Stibal R, Windscheif J and Jantz W** (1991) Contactless evaluation of semi-insulating GaAs wafer resistivity using the time-dependent charge measurement. *Semiconductor Science and Technology* **6**(10), 995. https://doi.org/10.1088/0268-1242/6/10/008

70. **Gao Y, Chen M, Yin S, Ruffin P, Brantley C and Edwards E** (2011) Terahertz enhancement from terahertz-radiation-assisted large aperture photoconductive antenna. *Journal of Applied Physics* **109**(3), 033108. https://doi.org/10.1063/1.3544044

71. **Shen YC, Upadhya PC, Beere HE, Linfield EH, Davies AG, Gregory IS, Baker C, Tribe WR and Evans MJ** (2004) Generation and detection of ultrabroadband terahertz radiation using photoconductive emitters and receivers. *Applied Physics Letters* **85**(2), 164–166. https://doi.org/10.1063/1.1768313

72. **Pozar DM** (2012) *Microwave Engineering*, 4th Edn. Hoboken, New Jersey: John Wiley & Sons.

73. **Vieweg N, Mikulics M, Scheller M, Ezdi K, Wilk R, Hubers HW and Koch M** (2008) Impact of the contact metallization on the performance of photoconductive THz antennas. *Optics Express* **16**(24), 19695–19705. https://doi.org/10.1364/OE.16.019695

74. **Tamagnone M, Gomez-Diaz JS, Mosig JR and Perruisseau-Carrier J** (2012) Analysis and design of terahertz antennas based on plasmonic resonant graphene sheets. *Journal of Applied Physics* **112**(11), 114915. https://doi.org/10.1063/1.4768840

75. **Dragoman M, Muller AA, Dragoman D, Coccetti F and Plana R** (2010) Terahertz antenna based on graphene. *Journal of Applied Physics* **107**(10), 104313. https://doi.org/10.1063/1.3427536

76. **Heshmat B, Pahlevaninezhad H, Darcie TE and Papadopoulos C** (2010) Evaluation of carbon nanotubes for THz photomixing. In *2010 IEEE Radar Conference*, Arlington, VA, USA.

77. **Fei Z, Rodin AS, Andreev GO, Bao W, McLeod AS, Wagner M, Zhang LM, Zhao Z, Thiemens M, Dominguez G, Fogler MM, Neto AHC, Lau CN, Keilmann F and Basov DN** (2012) Gate-tuning of graphene plasmons revealed by infrared nano-imaging. *Nature* **487**, 82–85. https://doi.org/10.1038/nature11253

78. **Freitag M, Low T, Zhu W, Yan H, Xia F and Avouris P** (2013) Photocurrent in graphene harnessed by tunable intrinsic plasmons. *Nature Communications* **4**, 1–8. https://doi.org/10.1038/ncomms2951

79. **Brar VW, Sherrott MC, Jang MS, Kim S, Kim L, Choi M, Sweatlock LA and Atwater HA** (2015) Electronic modulation of infrared radiation in graphene plasmonic resonators. *Nature Communications* **6**, 1–7. https://doi.org/10.1038/ncomms8032

80. **Masyukov M, Vozianova A, Grebenchukov A, Gubaidullina K, Zaitsev A and Khodzitsky M** (2020) Optically tunable terahertz chiral metasurface based on multi-layered graphene. *Scientific Reports* **10**, 3157. https://doi.org/10.1038/s41598-020-60097-0

81. **Milovanovic SP and Peeters FM** (2018) Strained graphene structures: from valleytronics to pressure sensing. In Bonča J, and Kruchinin S (eds.), Nanostructured Materials for the Detection of CBRN. *NATO Science for Peace and Security Series A: Chemistry and Biology*. Dordrecht, Netherlands: Springer, pp. 3–17. https://doi.org/10.1007/978-94-024-1304-5_1

82. **Liu J-X, Xie X, Du P, Liu Y-J and Yang H-W** (2019) Effect of graphene on the sunlight absorption rate of silicon thin film solar cells. *Plasmonics* **14**(2), 353. https://doi.org/10.1007/s11468-018-0811-6

83. **Wang S-Y, Zhang T, Yin W-Y and Zhou L**, "Interaction of electromagnetic waves with multilayer bi-anisotropic graphene structure," in 2013 USNC-URSI Radio Science Meeting (Joint with AP-S Symposium), Lake Buena Vista, USA, 2013.

84. **Shao Y, Yang -J-J and Huang M** (2016) A review of computational electromagnetic methods for graphene modeling. *International Journal of Antennas and Propagation* **2016**, 1–9. https://doi.org/10.1155/2016/7478621

85. **Wang X-H, Yin W-Y and Chen Z** (2015) Broadband modeling surface plasmon polaritons in optically pumped and curved graphene structures with an improved leapfrog ADI-FDTD method. *Optics Communications* **334**, 152–155. https://doi.org/10.1016/j.optcom.2014.08.038

86. **Bouzianas GD, Kantartzis NV, Antonopoulos CS and Tsiboukis TD** (2012) Optimal modeling of infinite graphene sheets via a class of generalized FDTD schemes. *IEEE Transactions on Magnetics* **48**(2), 379–382. https://doi.org/10.1109/TMAG.2011.2172778

87. **Nayyeri V, Soleimani M and Ramahi OM** (2013) Modeling graphene in the finite-difference time-domain method using a surface boundary condition. *IEEE Transactions on Antennas and Propagation* **61**(8), 4176–4182. https://doi.org/10.1109/TAP.2013.2260517

88. **Nayyeri V, Soleimani M and Ramahi OM** (2013) Wideband modeling of graphene using the finite-difference time-domain method. *IEEE Transactions on Antennas and Propagation* **61**(12), 6107–6114. https://doi.org/10.1109/TAP.2013.2282535

89. **Lin H, Pantoja MF, Angulo LD, Alvarez J, Martin RG and Garcia SG** (2012) FDTD modeling of graphene devices using complex conjugate dispersion material model. *IEEE Microwave and Wireless Components Letters* **22**(12), 612–614. https://doi.org/10.1109/LMWC.2012.2227466

90. **Wang D-W, Zhao W-S, Gu X-Q, Chen W and Yin W-Y** (2015) Wideband modeling of graphene-based structures at different temperatures using hybrid FDTD method. *IEEE Transactions on Nanotechnology* **14**(2), 250–258. https://doi.org/10.1109/TNANO.2014.2387576

91. **Brar VW, Jang MS, Sherrott M, Lopez JJ and Atwater HA** (2013) Highly confined tunable mid-infrared plasmonics in graphene nanoresonators. *Nano Letters* **13**(6), 2541–2547. https://doi.org/10.1021/nl400601c

92. **Yang J, Yang J, Deng W, Mao F and Huang M** (2015) Transmission properties and molecular sensing application of CGPW. *Optics Express* **23**(25), 32289–32299. https://doi.org/10.1364/OE.23.032289

93. **Burghignoli P, Araneo R, Lovat G and Hanson G** (2014) Space-domain method of moments for graphene nanoribbons. In Proceedings of the 8th European Conference on Antennas and Propagation (EuCAP '14), Hague, Netherlands.

94. **Araneo R, Burghignoli P, Lovat G and Hanson GW** (2015) Modal propagation and crosstalk analysis in coupled graphene nanoribbons. *IEEE Transactions on Electromagnetic Compatibility* **57**(4), 726–733. https://doi.org/10.1109/TEMC.2015.2406072

95. **Fallahi A, Low T, Tamagnone M and Perruisseau-Carrier J** (2015) Nonlocal electromagnetic response of graphene nanostructures. *Physical Review B* **91**, 121405. https://doi.org/10.1103/PhysRevB.91.121405

96. **Ryzhii V, Dobinov AA, Otsuji T, Mitin V and Shur MS** (2010) Terahertz lasers based on optically pumped multiple graphene structures with slot-line and dielectric waveguides. *Journal of Applied Physics* **107**(5), 054505. https://doi.org/10.1063/1.3327212

97. **Vasko FT and Ryzhii V** (2008) Photoconductivity of intrinsic graphene. *Physical Review B* **77**(19), 195433. https://doi.org/10.1103/PhysRevB.77.195433

98. **Dubinov AA, Aleshkin VY, Mitin V, Otsuji T and Ryzhii V** (2011) Terahertz surface plasmons in optically pumped graphene structures. *Journal of Physics Condensed Matter* **23**(14), 145302. https://doi.org/10.1088/0953-8984/23/14/145302

99. **Zolfagharloo-Koohi M and Neshat M**, "Antenna efficiency in graphene-based THz photoconductive antennas," in 2014 22nd Iranian Conference on Electrical Engineering (ICEE), Tehran, Iran, 2015.

100. **Emadi R, Emadi H, Emadi R, Safian R and Nezhad AZ** (2018) Analysis and design of photoconductive antenna using spatially dispersive graphene strips with parallel-plate configuration. *IEEE Journal of Selected Topics in Quantum Electronics* **24**(2), 1–9. https://doi.org/10.1109/JSTQE.2017.2693261

101. **Alharbi AG and Sorathiya V** (2022) Ultra-wideband graphene-based micro-sized circular patch-shaped Yagi-like MIMO antenna for terahertz

wireless communication. *Electronics* **11**(9), 1305. https://doi.org/10.3390/electronics11091305

102. **Amlashi SB, Khalily M, Singh V, Xiao P, Carey JD and Tafazolli R** (2021) Surface electromagnetic performance analysis of a graphene-based terahertz sensor using a novel spectroscopy technique. *IEEE Journal on Selected Areas in Communications* **39**(6), 1797–1816. https://doi.org/10.1109/JSAC.2021.3071835

103. **Abadal S, Hosseininejad SE, Cabellos-Aparicio A and Alarcon E** (2017) Graphene-Based terahertz antennas for area-constrained applications. In 2017 40th International Conference on Telecommunications and Signal Processing (TSP), Barcelona, Spain.

104. **Hanson GW** (2008) Dyadic Green's functions and guided surface waves for a surface conductivity model of graphene. *Journal of Applied Physics* **103**(6), 064302. https://doi.org/10.1063/1.2891452

105. **Gusynin VP, Sharapov SG and Carbotte JP** (2007) Magneto-optical conductivity in Graphene. *Journal of Physics: Condensed Matter* **19**, 026222.

106. **Wu H, Zhang J, Lian S, Wang B, Zheng L, Ye C and Wang G** (2024) High-performance 3D-graphene/GaAs photodetectors for applications in logic devices and imaging sensing. *IEEE Electron Device Letters* **45**(7), 1245–1248. https://doi.org/10.1109/LED.2024.3403982

107. **Thomson MD, Ludwig F, Holstein J, Al-Mudhafar R, Al-Daffaie S and Roskos HG** (2024) coherent terahertz detection via ultrafast dynamics of hot dirac fermions in graphene. *ACS Nano* **18**(6), 4765–4774. https://doi.org/10.1021/acsnano.3c08731

108. **Xiao L, Degl' Innocenti R and Wang Z** (2024) Key factors in achieving high responsivity for graphene-based tera-hertz detection. *Advanced Photonics Research* **5**(8), 2300272. https://doi.org/10.1002/adpr.202300272

109. **Joint F, Zhang K, Poojali J, Lewis D, Pedowitz M, Jordan B, Prakash G, Ali A, Daniels K, Myers-Ward RL, Murphy TE and Drew HD** (2024) Terahertz antenna impedance matched to a graphene photodetector. *ACS Applied Electronic Materials* **6**(6), 4819–4825. https://doi.org/10.1021/acsaelm.4c00870

110. **Zhou Q, Qiu Q and Huang Z** (2023) Graphene-based terahertz optoelectronics. *Optics & Laser Technology* **157**, 108558. https://doi.org/10.1016/j.optlastec.2022.108558

111. **Afsar MV and Button KJ** (1984) Millimeter wave dielectric properties of materials. In Button K J (eds.), *Infrared and Millimeter Waves*, Vol. 12, pp. 23-31. Orlando: Academic Press. chapter 1.

112. **PCA-Photocontuctive Antenna** (2022) BATOP Optoelectronics, [Online]. Available: https://www.batop.de/information/PCA_infos.html. [Accessed 8 Sep 2022].

113. **Filipovic DF, Gearhart SS and Rebeiz GM** (1993) Double-slot antennas on extended hemispherical and elliptical silicon dielectric lenses. *IEEE Transactions on Microwave Theory and Techniques* **41**(10), 1738–1749. https://doi.org/10.1109/22.247919

114. **Zmuidzinas J** (1991) Quasi-optical slot antenna SIS mixers. *IEEE Transactions on Microwave Theory and Techniques* **40**(9), 1797–1804. https://doi.org/10.1109/22.156607

115. **Gearhart SS and Rebeiz GM** (1994) A monolithic 250 GHz Schottky-diode receiver. *IEEE Transactions on Microwave Theory and Techniques* **42**(12), 2504–2511. https://doi.org/10.1109/22.339789

116. **Zhu N and Ziolkowski RW** (2013) Photoconductive THz antenna designs with high radiation efficiency, high directivity and high aperture efficiency. *IEEE Transactions on Terahertz Science and Technology* **3**, 721–730. https://doi.org/10.1109/TTHZ.2013.2285568

117. **Krysl A, But D, Ikamas K, Holstein J, Shevchik-Shekera A, Roskos H and Lisauskas A** (2024) Si superstrate lenses on patch-antenna-coupled TeraFETs: NEP optimization and frequency fine-tuning. *IEEE Sensors Journal* **24**(21), 33872–33880. https://doi.org/10.1109/JSEN.2024.3445140

118. **Yardimci NT and Jarrahi M** (2022) Nanostructure-enhanced photoconductive terahertz emission and detection. *Nano Micro Small* **14**(14), 1802437.

119. **Jiang L, Sun Y, Nowak C, Kibrom A, Zou C, Ma J, Fuchs H, Li S, Chi L and Chen X** (2011) Patterning of plasmonic nanoparticles into multiplexed one-dimensional arrays based on spatially modulated electrostatic potential. *ACS Nano* **5**(10), 8288–8294. https://doi.org/10.1021/nn202967f

120. **Berry CW and Jarrahi M** (2012) Terahertz generation using plasmonic photoconductive gratings. *New Journal of Physics* **14**, 105029. https://doi.org/10.1088/1367-2630/14/10/105029

121. **Lepeshov S, Gorodetsky A, Krasnok A, Rafailov E and Belov P** (2017) Enhancement of terahertz photoconductive antenna operation by optical nanoantennas. *Laser & Photonics Reviews* **11**(1), 1600199.

122. **Seniutinas G, Gervinskas G, Constable E, Krotkus A, Molis G, Valusis G, Lewis RA and Juodkazis S** (2013) THz photomixer with a 40nm-wide nanoelectrode gap on low-temperature grown GaAs. *Micro/Nano Materials, Devices, and Systems* **8923**, 301-309.

123. **Dionne JA, Sweatlock LA, Atwater HA and Polman A** (2005) Planar metal plasmon waveguides: Frequency-dependent dispersion, propagation, localization, and loss beyond the free electron model. *Physical Review B* **72**(7), 075405. https://doi.org/10.1103/PhysRevB.72.075405

124. **Heshmat B, Pahlevaninezhad H, Pang Y, Masnadi-Shirazi M, Lewis RB, Tiedje T, Gordon R and Darcie TE** (2012) Nanoplasmonic terahertz photoconductive switch on GaAs. *Nano Letters* **12**(12), 6255–6259. https://doi.org/10.1021/nl303314a

125. **Ishi T, Fujikata J, Makita K, Baba T and Ohashi K** (2005) Si nano-photodiode with a surface plasmon antenna. *Japanese Journal of Applied Physics* **44**, L364.

126. **Tang L, Kocabas SE, Latif S, Okyay AK, Ly-Gagnon D-S, Saraswat KC and Miller DA** (2008) Nanometre-scale germanium photodetector enhanced by a near-infrared dipole antenna. *Nature Photonics* **2**(4), 226–229. https://doi.org/10.1038/nphoton.2008.30

127. **Dintinger J, Robel I, Kamat PV, Genet C and Ebbesen TW** (2006) Terahertz all-optical molecule- plasmon modulation. *Advanced Materials* **18**, 1645–1648. https://doi.org/10.1002/adma.200600366

128. **Berry CW, Moore J and Jarrahi M** (2011) Design of reconfigurable metallic slits for terahertz beam modulation. *Optics Express* **19**(2), 1236–1245. https://doi.org/10.1364/OE.19.001236

129. **Unlu M, Hashemi MR, Berry CW, Li S, Yang S-H and Jarrahi M** (2014) Switchable scattering meta-surfaces for broadband terahertz modulation. *Scientific Reports* **16**(4), 5708.

130. **Unlu M and Jarrahi M** (2014) Miniature multi-contact MEMS switch for broadband terahertz modulation. *Optics Express* **22**(26), 32245–32260. https://doi.org/10.1364/OE.22.032245

131. **Hashemi MRM, Yang S-H, Wang T, Sepulveda N and Jarrahi M** (2016) Electronically-controlled beam-steering through vanadium dioxide metasurfaces. *Scientific Reports* **6**, 35439. https://doi.org/10.1038/srep35439

132. **Lepeshov S, Gorodetsky A, Krasnok A, Toropov N, Vartanyan TA, Belov P, Alu A and Rafailov EU** (2018) Boosting terahertz photoconductive antenna performance with optimised plasmonic nanostructures. *Scientific Reports* **8**, 6624. https://doi.org/10.1038/s41598-018-25013-7

133. **Pendry JB** (2008) Time reversal and negative refraction. *Science* **322**(5898), 71–73. https://doi.org/10.1126/science.1162087

134. **Web IS** 2012) Plasmonics: Merging photonics. *Science* **189**, 189–194.

135. **Ebbesen TW, Lezec HJ, Ghaemi HF, Thio T and Wolff PA** (1998) Extraordinary optical transmission through sub-wavelength hole arrays. *Nature* **391**, 667–669. https://doi.org/10.1038/35570

136. **Schuller JA, Barnard ES, Cai W, Jun YC, White JS and Brongersma ML** (2010) Plasmonics for extreme light concentration and manipulation. *Nature Materials* **9**, 193–204. https://doi.org/10.1038/nmat2630

137. **Genet C and Ebbesen TW** (2007) Light in tiny holes. *Nature* **445**, 39–46. https://doi.org/10.1038/nature05350

138. **Park S-G, Jin KH, Yi M, Ye JC, Ahn J and Jeong K-H** (2012) Enhancement of terahertz pulse emission by optical nanoantenna. *ACS Nano* **6**(3), 2026–2031. https://doi.org/10.1021/nn204542x

139. **Park S-G, Choi Y, Oh Y-J and Jeong K-H** (2012) Terahertz photoconductive antenna with metal nanoislands. *Optics Express* **20**(23), 25530–25535. https://doi.org/10.1364/OE.20.025530

140. **Jooshesh A, Smith L, Masnadi-Shirazi M, Bahrami-Yekta V, Tiedje T, Darcie TE and Gordon R** (2014) Nanoplasmonics enhanced terahertz

sources. *Optics Express* **22**(23), 27992–28001. https://doi.org/10.1364/OE.22.027992

141. **Amlashi SB, Khalidy M, Brown T, Xiao P and Tafazolli R**, An efficient plasmonic photoconductive antenna for terahertz continuous-wave applications. In *2021 15th European Conference on Antennas and Propagation*, Dusseldorf, German, 2021.

142. **Jooshesh A, Bahrami-Yekta V, Zhang J and Tiedje T** (2015) Plasmon-enhanced below bandgap photoconductive terahertz generation and detection. *Nano Letters* **15**(12), 8306–8310. https://doi.org/10.1021/acs.nanolett.5b03922

143. **Jarrahi M**, "High-efficiency terahertz sources based on plasmonic contact electrodes," in *2015 IEEE MTT-S International Microwave Symposium*, Phoenix, AZ, USA, 2015.

144. **Khiabani N, Huang Y, Garcia-Munoz LE, Shen YC and Rivera-Lavado A** (2014) A novel sub-THz photomixer with nano-trapezoidal electrodes. *IEEE Transactions on Terahertz Science and Technology* **4**(4), 501–508. https://doi.org/10.1109/TTHZ.2014.2320824

145. **Berry CW, Hashemi MR, Preu S, Lu H, Gossard AC and Jarrahi M** (2014) High power terahertz generation using 1550 nm plasmonic photomixers. *Applied Physics Letters* **7**(104), 011121.

146. **Heshmat B, Masnadi-Shirazi M, Lewis RB, Zhang J, Tiedje T, Gordon R and Darcie TE** (2013) Enhanced terahertz bandwidth and power from GaAsBi-based sources. *Advanced Optical Materials* **1**(10), 714–719. https://doi.org/10.1002/adom.201300190

147. **Krotkus A, Arlauskas A and Adomavicius R** (2012) Semiconductor investigation by terahertz radiation pulses. *Proceedings of SPIE, 8496, Terahertz Emitters, Receivers, and Applications III*, 84960V. (15 October 2012). https://doi.org/10.1117/12.929130

148. **Zhang X, Zhan F, Wei X, He W and Ruan C** (2021) Performance enhancement of photoconductive antenna using saw-toothed plasmonic contact electrode. *Electronics* **10**(21), 2693–2702. https://doi.org/10.3390/electronics10212693

149. **Birks TA, Knight JC and Russell PS** (1997) Endlessly single-mode photonic crystal fiber. *Optics Letters* **22**, 961–963. https://doi.org/10.1364/OL.22.000961

150. **Rahmati E and Ahmadi-Boroujeni M** (2019) Design of terahertz photoconductive antenna arrays based on defective photonic crystal substrates. *Optics & Laser Technology* **114**, 89–94. https://doi.org/10.1016/j.optlastec.2019.01.044

Ruobin Han is a PhD candidate at the University of Glasgow, specializing in terahertz photoconductive antennas and nanophotonic device design. His work focuses on performance enhancement strategies in THz systems using novel materials and antenna geometries.
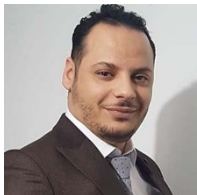
Dr. Abdoalbaset Abohmra is a researcher at the University of Glasgow. His research interests include microwave engineering, THz system integration, and antenna simulation techniques.

Tomas Pires is currently a PhD candidate at the University of Glasgow. His expertise lies in electromagnetic simulations, antenna design, and THz biomedical applications.

Prof. Joao Ponciano is a Senior Lecturer and Vice-Dean for the Glasgow College transnational partnership between University of Glasgow and University of Electronics Science and Technology of China. His research interests include networking systems and technologies, distributed systems and cybersecurity, relational database systems, data mining, simulation modelling and data analytics and software engineering design and development.

Dr. Hasan Abbas is a researcher at the University of Glasgow, focusing on RF systems and antenna design. His current work includes THz sensors and their applications in healthcare and security.

Prof. Akram Alomainy is a Professor of Antennas and Applied EM at Queen Mary University of London. He is internationally recognized for his work in body-centric wireless communications, antennas, and THz technologies.

Dr. Farooq A. Tahir is with the University of Glasgow and COMSATS University Islamabad. His research spans terahertz systems, 5G/6G wireless technologies, and reconfigurable antenna design.

Prof. Muhammad Imran is the Head of the Communications, Sensing and Imaging Group at the University of Glasgow. He has extensive experience in wireless systems, with contributions to 5G, IoT, and THz communication.

Prof. Qammer Abbasi is a Professor at the James Watt School of Engineering, University of Glasgow. His research focuses on antennas, body-centric communications, and THz technologies for healthcare, sensing, and communication applications.